EUROPEAN ORGANIZATION FOR NUCLEAR RESEARCH

CERN-PPE/92-172
07.10.1992

Calibration and Performance of the CHARM-II Detector

The CHARM-II Collaboration

D. Geiregat[1], **P. Vilain**[2], **G. Wilquet**[2]
Inter-University Institute for High Energies (ULB-VUB), Brussels, Belgium.

U. Binder[3], **H. Burkard**, **W. Flegel**, **H. Grote**, **T. Mouthuy**[4], **H. Øverås**, **J. Panman**, **A. Rozanov**[5], **K. Winter**, **G. Zacek**, **V. Zacek**
CERN, Geneva, Switzerland

R. Beyer[6], **F.W. Büsser**, **C. Foos**, **L. Gerland**, **T. Layda**, **F. Niebergall**, **G. Rädel**[7], **P. Stähelin**, **A. Tadsen**[8], **T. Voss**
II. Institut für Experimentalphysik[9], *Universität Hamburg, Hamburg, Germany*

D. Favart, **G. Grégoire**, **E. Knoops**[1], **V. Lemaître**
Université Catholique de Louvain, Louvain-la-Neuve, Belgium

P. Gorbunov, **E. Grigoriev**, **V. Khovansky**, **A. Maslennikov**
Institute for Theoretical and Experimental Physics, Moscow, Russian Federation

W. Lippich, **A. Nathaniel**, **H. Neumeyer**, **A. Staude**, **J. Vogt**
Sektion Physik[9] *der Universität München, Munich, Germany*

M. Caria[10], **C. Cicalò**[10], **B. Eckart**[11], **A.G. Cocco**, **A. Ereditato**, **G. Fiorillo**, **S. Mennella**, **V. Palladino**, **P. Paolucci**, **P. Strolin**
Università e Istituto Nazionale di Fisica Nucleare (INFN), Naples, Italy

A. Capone, **D. De Pedis**, **E. Di Capua**[12], **U. Dore**, **A. Frenkel-Rambaldi**, **P.F. Loverre**, **D. Macina**, **G. Piredda**, **R. Santacesaria**, **D. Zanello**
Università 'La Sapienza' e Istituto Nazionale di Fisica Nucleare (INFN), Rome, Italy

submitted to Nucl. Inst. & Meth.

Abstract

The neutrino detector CHARM-II at CERN, consisting of a large target calorimeter, equipped with streamer tubes, and a muon spectrometer has been exposed to a test beam of electrons, pions and muons with momenta between 2 and 60 GeV/c in order to study the digital response of the streamer tubes, the analog response of the pickup strips and the momentum resolution of the muon spectrometer.

Methods have been developed to carry the calibration results in space from the impact point of the test beam to the bulk of the detector and in time from the test beam period to all the data taking periods between 1987 and 1991. The number of hits along muon tracks was used to parametrize the dependence on fluctuations of temperature, tube voltage and gas composition.

Curves and formulae are presented showing the energy response and the energy resolution for the different beam particles. The test beam data have been used to optimize and calibrate algorithms for the kinematical reconstruction of electron showers and for their extraction from the vast background of hadronic showers.

---

[1] Inter-University Institute for Nuclear Science, Belgium
[2] National Foundation for Scientific Research, Belgium
[3] now at University of Freiburg, F.R.G.
[4] now at Centre de Physique des Particules, Faculté de Luminy, Marseilles, France
[5] on leave of absence from ITEP, Moscow, Russian Federation
[6] now at CERN, Geneva, Switzerland.
[7] now at DESY, Hamburg, F.R.G.
[8] now at University of Neuchatel, Switzerland
[9] supported by the German Bundesministerium für Forschung und Technologie under contract numbers 05-4HH22P and 05-4MU12P.
[10] now at Università di Perugia, Italy
[11] now at University of Basel, Switzerland
[12] Dipartimento di Fisica, Università di Ferrara, Italy

1 Introduction

Neutrino physics continues to play an important and unique role in the investigation of the basic questions of elementary particle physics. In addition to the impressive successes of the Standard Model obtained in experiments performed at high energy $p\bar{p}$ and e^+e^- colliders, neutrino experiments offer the possibility of a complementary study of the neutral current sector of the Standard Model.

The CHARM-II collaboration, profiting from the experience gained in the earlier CHARM experiment [1, 2], has designed and built a new detector for operation in the wide-band neutrino beam of the CERN SPS. The main aim of the experiment is the determination of the weak mixing angle $\sin^2\theta_W$ using the scattering of muon neutrinos and muon antineutrinos off electrons. Signature for a neutrino electron scattering event is a single recoiling electron which is, because of its low mass, kinematically constrained to a strongly forward peaked cone with an opening angle θ_e given by the condition

$$E_e\theta_e^2 \leq 2m_ec^2. \quad (1)$$

At the mean energy $E_e \approx 10\,\mathrm{GeV}$ of recoiling electrons, θ_e is less than $\approx 10\,\mathrm{mrad}$.

One major challenge of the experiment is to extract neutrino-electron scattering events out of a 10 000 fold larger background which is due to neutrino scattering off nuclei. To distinguish hadronic and electromagnetic showers, different characteristics of the shower development, such as the lateral width and the energy density, can be exploited. By an appropriate choice of the target material and of the granularity of sensitive detector elements the required selection power can be achieved. The remaining electromagnetic part of the background due to neutrino-nucleon scattering can largely be rejected by a precise measurement of the kinematically invariant quantity $E\theta^2$ which, being governed by the nucleon mass, shows a much broader distribution. Furthermore, showers induced by the scattering of neutrinos on electrons start with one single electron at the vertex, which provides an additional constraint on the selection of events. Thus, for a reliable recognition of neutrino electron scattering events, the detector design has to provide means for measuring shower energy and shower direction and for identifying the event vertex.

To extract physics results from the measurements of neutrino interactions in the CHARM-II detector, the response to electrons and hadrons over a wide energy range and the distinct properties of the showers induced by these particles have to be studied. The exposure of the calorimeter to electron and pion test-beams of known energy allowed us to obtain the absolute energy response of the calorimeter and the characteristics of electron induced showers in comparision to hadronic showers.

For practical reasons only the front part of the long CHARM-II detector could be exposed to the test beams. Moreover, the test-beam was only available for a few weeks, which is short compared to the five years of data collection in the neutrino beam. A method was therefore required to apply the test-beam calibration to other parts of the detector and to other data taking periods. An ideal source to continuously monitor the detector response are cosmic ray muons which were recorded, in parallel to neutrino data taking, inbetween two successive neutrino bursts. This reference sample can be used to correct globally for space and time dependent sensitivity variations. Because of energy dependent saturation effects this method, however, turned out to be not satisfactory when applied to electromagnetic showers. Thus, in addition, also neutrino-induced electromagnetic showers were used to carry the calibration result in space from the front end to the full detector and in time from the test beam exposure to other periods.

A first calibration of the CHARM-II detector had been performed in 1986. The analysis presented here is based on data taken in a test beam of electrons, pions and muons during October and November 1989. The test-beam data have been used to optimize the methods which were developed to distinguish electromagnetic and hadronic showers and to determine the energy and the direction of showers. Together with a detailed description of the CHARM-II detector [3], this paper is intended to help in the critical understanding of published [4, 5, 6] and of forthcoming physics results.

2 The CHARM-II neutrino detector

The design of the CHARM-II detector is optimized to obtain good angular resolution and efficient electron-hadron separation. This led to the realization of a highly granular structure of active detector elements, giving the possibility of frequent shower sampling and the choice of low Z target material to reduce the effects of multiple scattering. In addition a large fiducial mass is mandatory to collect a statistically significant sample of neutrino-electron scattering events despite the very small reaction cross section $\sigma/E \sim 2 \times 10^{-42} cm^2/GeV$.

The detector layout is shown in fig. 1. It consists of a target calorimeter, 36 m long, with a square cross section of 3.7 m x 3.7 m and with a total mass of 692 tons. It is centered along the neutrino beam axis and is followed by a magnetized iron spectrometer used for the momentum analysis of penetrating muons needed for the purpose of neutrino flux normalization. The target calorimeter is constructed out of 420 modules. Each module consists of a 4.8 cm thick glass target plate (Z=11), followed by a layer of plastic streamer tubes with 1 cm wire spacing. The tubes layers are instrumented with

2 cm wide pick-up strips oriented orthogonally to the direction of the wires. The wire signals are registered digitally, i. e. any signal exceeding a fixed discriminator level is counted and will subsequently be referred to as one hit. The charges induced on the pick-up strips are read out as analog signals. The orientation of the streamer tubes alternates in subsequent modules between vertical and horizontal. Thus, in one module, depending on the projection, either the hit distribution from the tubes or the charge distribution from the pick-up strips is observed. Every fifth module contains a layer of scintillators which is 3 cm thick and covers an area of 3 m × 3 m. In total the calorimeter contains 154 560 digital channels of the streamer tube system, 73 920 cathode pick-up strips multiplexed into 9 240 analog channels and 1 540 analog channels of the scintillator system.

The muon spectrometer[1] consists of six magnetized iron modules, each of which is equipped with four scintillator counter tube layers. Nine drift chambers, each containing three layers of wires in different orientations $(-60°, 0°, +60°)$, allow the reconstruction of the muon momentum from the track curvature.

A more detailed description of the individual detector elements can be found in [3].

Fig. 2 shows, in one of the two available projections, *(a)* a purely electromagnetic shower originating from a single incident electron and *(b)* a hadronic shower which is due to an incident pion from a test beam. Tube hits are visible as small dots in every second module. The analog signals from the interleaving tube layers are represented by small squares with an area proportional to the signal amplitude. It is evident that the differences between the two showers can easily be recognized. Electromagnetic showers are narrow and show a more or less regular evolution, while hadronic showers are wider and show a highly irregular structure.

3 Test-beam calibration

3.1 Layout of the test beam

To produce electrons and pions needed for the calibration of the detector a secondary particle beam from the SPS, containing electrons and pions with an energy of 135 GeV, is sent onto a copper or lead target. Depending on the target material chosen, a tertiary beam predominantly consisting of electrons or pions is produced. The low intensity tertiary test beam X7 used for the present calibration covered a momentum range from 1 to 63 GeV/c. For beam momenta from 3 to 40 GeV/c the central beam momentum was known to better than ± 1 % and the momentum spread was 0.75 % at the smallest opening of the momentum slits. The particle beam was ejected in a spill of 2.4 s duration, followed by the short 6 ms burst of the neutrino beam. The beam intensity was kept below 100 particles per spill in order to allow for the readout of various beam monitoring devices in the available time.

Fig. 3 shows the layout of the test beam. The test beam passed through vacuum up to the last bending magnet (BM). This magnet allows to steer the beam to two different impact points (P1 and P2) on the calorimeter front face. This is important for studying the response of the detector to incident particles of different directions and to test at least two different positions of the detector. In position P1 the beam ran parallel to the calorimeter axis which coincided with the axis of the neutrino beam. In position P2 which lay 20 cm below the level of position P1, the beam formed an angle of 30 mrad with respect to the calorimeter axis. The quadrupole QP upstream of the bending magnet allowed horizontal focusing or defocusing of the beam, compromising thereby between the desirable maximization of the beam width and the minimization of scattering on limiting apertures.

Most of the distance between the bending magnet and the calorimeter is occupied by a 21.9 m long helium filled threshold Čerenkov counter which could be moved together with the beam, depending on the chosen impact point. Two more Čerenkov counters, filled with helium resp. nitrogen gas, are installed further upstream of the bending magnet. Depending on the selected beam energy the pressure of the Čerenkov counters was adjusted to keep good efficiency for the identification of electrons. A coincidence signal of all three Čerenkov counters reliably tagged electrons up to ≈ 40 GeV/c. At higher energies, electrons were distinguished from pions by their shower profile observed in the CHARM-II detector (cf. section 8).

A set of three halo counter hodoscopes (H1,H2,H3) encircled the beam line at different positions. One of these lead scintillator counters (H3) was mounted directly in front of the calorimeter while the remaining two counters were located further upstream in the beam line. Signals registerd in the halo counters served to reject particles having experienced an interaction in the beam line which may have affected their energy or direction.

Two beam defining scintillators (TA,TB), installed at the entrance and at the exit of the long Čerenkov, counter were used in the trigger logic to indicate the crossing of a particle. A valid beam event was defined by a coincidence signal from both scintillators being in anticoincidence with the signals from the halo counters.

To define the point of impact of the beam particle and its direction with high precision, the beam line was equipped with four multiwire chambers. These beam profile counters (BPC1 to BPC4)

[1] The main components of the muon spectrometer have kindly been lent to us by the CDHS collaboration.

were mounted in front and behind the 22 m long Čerenkov counter and achieved a precision of about 2 mm. The information from the beam profile counters was used to develop and optimize algorithms for the reconstruction of the shower vertex and of the shower direction.

3.2 Measurement conditions and test beam parameters

The calibration of the target calorimeter was performed in parallel to neutrino data taking. For this purpose the veto planes (see fig. 1), which precede the calorimeter, were moved sideways to allow the particle test beam to impinge onto the front end of the target calorimeter. The first glass plate of the target calorimeter had a hole of 20 cm diameter at the impact point P1. The gap between the first and the second target plate had been increased in order to leave room, behind the streamer tube layer, for a scintillator which could be moved in and out of the beam. This scintillator was used to study the energy deposition E_{first} at the beginning of an electron-induced shower, with the aim to distinguish it from a shower due to the decay of a π^o into two gammas. From the second plate onwards the calorimeter remained in its regular structure.

With the hole in position P1 open, showers started in a tube layer with vertical tubes. In order to study the effect of possible asymetries between the performance of vertical and horizontal detector elements, an additional streamer tube layer with horizontal wires could be mounted in front of the first glass plate. In this case the hole in the plate was refilled with its glass core.

To simulate the uniform probability of neutrino interactions at any depth within a glass target plate, an array of triangular aluminum wedges was mounted between the beam scintillator TB and the halo counter H3. The height of the wedges was chosen to be equivalent to the thickness of a target plate when expressed in units of radiation lengths. The base width of the wedges, 5 mm, was small compared to the beam size. Incoming beam particles, therefore, had uniform probability of traversing between 0 mm and 42 mm of aluminum before reaching the the first tube layer.

When the particle beam was directed to the impact points P1 or P2 Čerenkov-flagged electrons or pions with beam momenta 1, 2, 2.5, 3, 4, 6, 8, 10, 15, 20, 25, 30, 35 and 40 GeV/c were measured. These momentum values safely included the energy range of 3 GeV to 24 GeV used in the analysis of neutrino-electron scattering. For higher momenta the bending power of the magnet was insufficient to steer the beam to position P1; therefore measurements with beam momenta 50, 55 and 63 GeV/c were taken only at position P2.

Variations in the applied streamer tube voltage influence the determination of the shower energy and the event selection efficiencies. To study these effects test beam data were taken for which the nominal voltage of 4300 V was systematically varied by ± 30 V and ± 60 V.

The muon spectrometer was calibrated using muons with a momentum of 60 GeV/c. The muon beam was obtained by selecting in the X7 tertiary beam the 60 GeV decay products of 100 GeV secondary pions. Its calculated momentum spread was $\Delta p/p \approx 3\,\%$ and the uncertainity in the absolute scale was $\pm 1\,\%$.

4 Calibration of the streamer tube system

4.1 A new method to monitor the streamer tube response

Cosmic-ray muons provide a perfect source for monitoring the long-time performance of the detector. During normal data taking, 10 cosmic-ray events were recorded per accelerator cycle, yielding 25 000 events per ten hours. During test-beam operations, when the detector conditions were changed frequently, the rate of cosmic-ray muons recorded was increased to allow monitoring of the behaviour of the detector in steps of about three hours.

Only events for which the muon track could be reconstructed in both projections have been used for calibration and monitoring purposes. Events showing several tracks or a bremsstrahlung shower along the track were rejected. The cosmics trigger required a penetration of at least $\approx$ 110 modules and thus selected rather flat cosmics with a direction deviating at most 22° from the calorimeter axis

These cosmic rays and high-energy muons accompanying the neutrino beam have been used to measure the precise alignment of the streamer tubes. For the position of the streamer tubes a precision of ± 0.3 mm has been obtained.

The voltage applied to the streamer tubes has a direct impact on their response: with increasing voltage more and more particles traversing only a small part of a tube, e. g. delta rays crossing a corner only, get a chance to induce a complete streamer. Moreover, cross-talk effects simulating additional hits become more important with increasing voltage. In addition, the response of the streamer tubes is affected by the gas pressure (correlated with the atmospheric pressure), by the gas temperature and by the gas composition. In order to compensate variations of these parameters a feed-back-loop system had been installed (see ref. [3], p. 675). While the correction for pressure variations proved to be fully satisfactory, the compensation for temperature fluctuations worked for a specific location only. Over the full length of the detector, temperature differences were unavoidable

and changed with time. As a result of these variations and because of manual adjustments of the nominal tube voltage between data-taking periods, the response of the streamer tube system showed a dependence on time as well as on the longitudinal calorimeter coordinate.

This led to the development af a method to correct for position and time dependent fluctuations of the tube response. As a first step we had to find an observable which allowed continuous and reliable monitoring of the tube sensitivity. Among several possibilities, the average multiplicity α_{mult} of hits along cosmic muon tracks was chosen as the observable to be monitored. The probability that a short delta-ray or a primary track crossing only a corner of a tube triggers a detectable streamer depends on the gas composition, the gas pressure, the temperature and the tube voltage and is a useful indicator of tube sensitivity.

Before this multiplicity can be used, two corrections must be applied. The first correction is necessary because the directional distribution of accepted cosmic rays is not exactly the same in all parts of the detector. The probability of one or more hits being registered in a given tube layer depends on the direction of the track. Tracks which are orthogonal to a tube layer have about 11 % probability of beeing invisible in this particular layer, because they can traverse the layer entirely inside a wall separating two tubes. If the slope of a track (as measured in plane which is orthogonal to the direction of the tubes) increases, the probability of it being invisible decreases and the probability of penetrating two adjacent tubes grows. This dependence on the the track slope has been measured (fig. 4) and is used to reduce the observed hit multiplicities to a nominal hit multiplicity refering to tracks which are normal to the tube layers.

The second correction compensates variations of the hit multiplicity as a function of the position along the tubes. In comparision to the multiplicity at the read-out end of the tube, the multiplicity was found to be about 10 % higher at the far end of the tube. This effect is mostly due to cross-talk via the high-resistivity cover which is common to eight adjacent streamer tubes. Hence, it depends on the distance the signal travels along the wire towards the read-out end [2]. The correction is performed on the basis of the curve shown in fig. 5.

The result of the two corrections is a *normalized hit multiplicity* $\alpha_{\text{mult}}(x,t)$ which characterizes the sensitivity of the tubes as a function of space and time. The values of α_{mult} happen to be close to 1.0 because the loss due to 'invisible' tracks is approximately compensated by extra hits due to delta rays.

[2] A posteriori, it was found that the effect could have been reduced to a negligible level by an improvement of the ground return.

4.2 Parametrisation of the tube sensitivity by an effective tube voltage

For practical applications the normalized hit multiplicity was converted to a variable which is accessible to a more direct control during test-beam operation. An 'effective tube voltage' U_{eff} has been defined as a function of the normalized hit multiplicity by the equation

$$U_{\text{eff}} = 4300\ \text{V} + (\alpha_{\text{mult}} - 1.006) \cdot 1808\ \text{V} \qquad (2)$$

The effective voltage is, to a close approximation, the tube voltage which produces at some reference condition of the detector (pressure 1019 mb and temperature 23° C) the normalized multiplicity α_{mult}. Fig. 6 shows for test-beam muons the observed relation between hit multiplicity and tube voltage under reference conditions of the detector. In the remainder of this report, instead of α_{mult}, the dependent variable $U_{\text{eff}}(\alpha_{\text{mult}})$ will be used as a measure of tube sensitivity.

An average value of the 'effective tube voltage' U_{eff} was determined for each group of 20 modules for each period of about one week. Shorter periods were adopted if necessary. Typically about 25 000 cosmic-ray muons entered in the determination of one set of effective voltages. Fig. 7 shows the effective tube voltage averaged over the full detector as a function of time. The variation of U_{eff} along the detector axis is shown fig. 8 for one period middle of June 1988.

The tube sensitivity, which is parametrized bymeans of the effective voltage, will enter the determination of the shower energy performed on the basis of the recorded number of hits. In addition, it has to be included in the evaluation of event selection efficiencies. Variations of the tube voltage during the test-beam operation allowed to study how the energy response and the selection efficiencies depended on the tube voltage. The knowledge of the effective tube voltage for each group of detector modules in each period led to a determination of energy and selection efficiencies which were independent of time and space over the five years.

4.3 Energy of electromagnetic showers from the number of active tubes

The determination of the energy of eletromagnetic showers using the streamer tubes is based on the observed number of hits in the first 30 tube layers of the shower. Laterally, only tubes within a distance of less than 25 cm from the shower axis are included.

For test-beam electrons of different energies, the relation between the number of hits N observed and the energy E_e of the incident electron is shown in fig. 9 and is parametrized as:

$$E_e = \left(\frac{N + 36.7}{57.5}\right)^{1.83}\ \text{GeV}. \qquad (3)$$

To transport this calibration to other parts of the detector and to other periods of time, the then observed number of hits N_{obs} has to be corrected to match the standard operating conditions of the test beam period. This is done by using for each group of 10 modules the corresponding specific value of the effective voltage previously determined with the help of cosmic ray muons. The resulting correction factor which has to be applied to the observed number of hits shows the following dependence on U_{eff}:

$$F_e(U_{eff}) = 1.00 - 0.14 \times (U_{eff} - 4300\text{V})/(100\,\text{V})$$

It has been found that this correction is to a good approximation independent of the shower energy.

In addition, one has to correct for cross talk effects. Due to cross talk between individual streamer tubes, the number of active tubes in a shower depends on the distance v of the shower from the read-out end. However, the number of active profiles is not sensitive to the shower position. (A profile is a group of eight adjacent streamer tubes under a common high-resistivity cover; it is said to be active when there is at least one tube hit.) The average ratio of active tubes to active profiles can therefore be used to derive a correction factor $P(v)$ which takes care of cross-talk effects. Refering to a shower in a central position, the correction amounts to about $+10\%$ and -10% respectively at both ends of the tubes.

The combination of the two corrections converts the obseved number of hits to the number N expected under standard conditions of the detector and accounts for cross talk effects:

$$N = F_e(U_{eff}) \times P(v) \times N_{obs}$$

Inserting this value into eq.(3) yields the energy of the electromagnetic shower. In the energy range 2 to 40 GeV which includes the energies used in the analysis of neutrino-electron scattering, the absolute scale error of this energy determination is estimated to be $\leq 5\%$. A fit to the energy resolution in the range 3 to 40 GeV yields

$$\sigma(E_e)/E_e = 0.09 + 0.15/\sqrt{E_e/\text{GeV}} \qquad (4)$$

4.4 Energy of pion-induced hadronic showers

For a safer selection of pions, beyond the tagging in the Čerenkov counters, only pions were accepted wich showed a clearly visible incoming track in the first modules of the calorimeter. The number N of accepted tube hits was not restricted by any geometrical cut and did not include the hits caused by the incoming pion before the hadronic interaction. To obtain the energy of the hadronic shower E_π, the energy loss of the pion between its point of entrance into the calorimeter and the shower vertex was subtracted from the nominal beam energy.

In the energy range 2 to 60 GeV the relation observed between the number of hits generated by test-beam pions and the hadronic energy is shown in fig. 10 and can be described by:

$$N = 27.7 \cdot (E_\pi/\text{GeV})^{0.863} - 16.8 \qquad (5)$$

As in the case of electromagnetic showers a correction factor depending on the effective voltage has to be applied to the observed number of hits when the test-beam calibration is transported to different time periods and to other parts of the detector. The correction factor is given by:

$$F_\pi(U_{eff}) = 1.0 - 0.10 \cdot (U_{eff} - 4300\text{V})/(100\text{V})$$

The correction which is expressed in this factor is smaller than in the case of electrons (eq. 4.3) because electromagnetic showers are denser and, due to higher charges in the shower core, more likely to produce extra hits via crosstalk.

The observed energy resolution in the energy range from 2 to 60 GeV can be parametrized as

$$\sigma(E_\pi)/E_\pi = 0.07 + 0.31/\sqrt{E_\pi/\text{GeV}}. \qquad (6)$$

4.4.1 Neutrino-induced hadronic showers

One aim of the CHARM-II experiment is the investigation of neutrino- induced events with two outgoing muons. Most of these events are generated via the production and the decay of D-mesons. For the analysis of these dimuon events, one needs to know the response of the detector to hadronic showers produced by semileptonic neutrino interactions. Hadronic showers due to neutrino interactions differ from pion-induced showers in their particle composition and in their opening angle.

The Lund Monte-Carlo program[3] was used to generate dimuon events. The response of the detector to each secondary particle, was simulated and superimposed using the GEANT Monte-Carlo program, which had been extended and fine-tuned to reproduce the response to test-beam electrons and pions, including position dependent crosstalk effects (see section 4.1) and 'satellite' hits due to soft photons below the cut-off energy used in the simulation.

To check the validity of this procedure, test beam events, pions and/or electrons, were superimposed by 'OR'ing their hits. The same combinations were generated with the Monte-Carlo program. A good agreement was found, and the results gave confidence in the Monte-Carlo simulation.

The result is a formula which yields, as a function of the number N of tube hits, the energy E_{cc} of hadronic showers produced in neutrino interactions. While this relation has been derived for the

[3] LEPTO version 5.2, July 31, 1987 in combination with JETSET version 6.3

special case of dimuon events, we believe that it holds in a good approximation for any hadronic showers produced in '*charged current*' reactions i. e. in reactions which change the incoming neutrino into an outgoing muon.

$$\frac{E_{cc}}{\mathrm{GeV}} = \frac{N}{18.69} \times \left(1 + \frac{N}{2980} - 0.056 \cdot \frac{U_{\mathrm{eff}} - 4300\mathrm{V}}{100\mathrm{V}}\right) \quad (7)$$

Again a correction has been included to take into account time and position dependent sensitivity fluctuations which are parametrized by U_{eff}.

The energy resolution is independent of the tube voltage:

$$\sigma(E_{cc})/E_{cc} = 0.02 + 0.52/\sqrt{E_{cc}/\mathrm{GeV}} \quad (8)$$

5 Calibration of the pick-up strip system

5.1 Response of the pickup strips to cosmic ray muons

Cosmic rays were used to study the response of the pickup strips to the charge induced by the streamers. Clean tracks traversing a streamer tube layer induce the highest charge directly on the strip the track traverses, and smaller satellite signals on neighbouring strips. For monitoring purposes, the 'cluster charge', i. e. the sum of the charges on three neighbouring strips closest to the track, was used.

It was found that the cluster charge shows a periodic dependence on the coordinate along the strips, reflecting the modular structure of the underlying streamer tubes (fig. 11). Each group of 8 tubes has a common high-resistivity cover between the gas volume and the pickup strips which run across the tubes. Tracks passing through a tube near the center of a group gave a charge smaller by $\approx 25\,\%$ than tracks passing through an edge tube. Superimposed is a slight modulo-16 periodicity, because two adjacent groups of eight tubes are mounted in a common envelope. These observed periodicities were used to apply corrections for the calibration of the average strip response.

For the analysis of our neutrino data in previous publications, only one average calibration constant per streamer tube layer was used. A more detailed mapping of the strip response within the tube layers led to a slight improvement in vertex and direction resolution. The response varies between individual strips (i) and depends on the underlying group of 8 tubes . It turns out that the response function can be factorized into a strip-dependent part s_i and a part t_j depending on the tubes. For each strip a separate calibration constant was determined, yielding a total of 73'920 calibration constants s_i for the full detector. The dependence of the response function on the underlying tubes is superimposed. Each group of 8 tubes was longitudinally subdivided into 4 sectors, and for each sector (j) the average response was measured. For the full calorimeter, this gave 73'920 additional constants t_j.

The multiplication of the raw cluster charge with the two calibration factors gives the corrected charge which enters the data analysis: $Q = s_{\mathrm{i}} \times t_{\mathrm{j}} \times Q_{\mathrm{raw}}$

Fig. 12 compares, for one particular tube layer, the raw cluster charge and the resulting corrected charge as a function of the strip number i, averaged over all underlying tubes. The fact that the distribution of corrected pulse heights is nearly flat gives an a-posteriori justification for the factorization of the calibration constants. A study of the long-time stability, using cosmic rays taken during the five years of data taking, has shown that it is sufficient to determine a new set of constants s_i and t_j every two months.

Penetrating cosmic rays have also been used to determine the exact position of the pickup strips. A slight curvature of the strips was found. In some few cases the extreme values of the sagitta amounted to 5 mm. As a consequence of the fabrication process, neighbouring strips showed a similar curvature, and it was sufficient to fit a common parabola to every group of eleven adjacent strips. For the full calorimeter the description of the strip shapes required $\approx$ 20 000 constants. With this parametrisation it was possible to reduce the uncertainity of the strip positions from about ± 4 mm to less than ± 2 mm. These corrections were used in the analysis of electromagnetic showers in order to improve the precision of the vertex location.

5.2 Energy of electromagnetic showers from the charge on the pickup strips

The energy of an electromagnetic shower can also be determined from the total charge induced on the pickup strips in the first 30 tube layers following the event vertex. Fig. 13 shows the dependence of this charge on the energy of test-beam electrons. The charge scale (ADC-channels per GeV) contains a factor A which cancels when neutrino induced showers are compared (this is the purpose of the calibration) to test-beam showers. Test-beam data, in the range from 2 to 40 GeV, can be fittet by the relation

$$Q(E) = \mathrm{A} \times E \times (1 - E/(220\,\mathrm{GeV})) + 0.16\,\mathrm{GeV} \quad (9)$$

The last term, a constant offset, is a consequence of the noise on the pickup strips. The energy resolution found in test-beam showers is

$$(\sigma(E_e)/E_e)_{\mathrm{TB}} = 0.034 + 0.24/\sqrt{E_e/\mathrm{GeV}} \quad (10)$$

To transport this calibration result in space and time, cosmic muons are not useful as a reference standard because they are not affected by charge

saturation effects which can be present in the core of showers. Instead, neutrino-induced events were used which passed all the selection criteria for electromagnetic showers (see section 8). Only the digital information of the streamer tubes was used for this selection. A careful study confirmed that these reference events were evenly distributed throughout the detector.

For each group (k) of 20 successive detector modules and for time slices (m) of about 1 month, the average charge $Q_{k,m}$ of these reference events was evaluated. The ratio $Q_{k,m}/Q_{1,\mathrm{TB}}$ was then used to carry the energy calibration from the first group of tube layers ($k = 1$) and the test-beam period ($m = \mathrm{TB}$) to other parts of the detector and to other data-taking periods.

This procedure suffers from statistical errors due to the limited number of available neutrino-induced reference showers per detector subdivision and time slice. The size of the statistical errors was estimated from the fluctuations which were observed when a finer subdivision of the sample was used. This adds a contribution $(\sigma(E_e)/E_e)_{\mathrm{transport}} = 0.042$ to the energy resolution. This contribution is largely independent of energy. Since both error sources are independent, their squares can be added in each energy bin.

The overall energy resolution determined from the charges induced on the pick-up strips is finally given by (fig. 14):

$$(\sigma(E_e)/E_e)_{\mathrm{TB}} = 0.05 + 0.23/\sqrt{E_e/\mathrm{GeV}} \quad (11)$$

The main contribution ($\pm 6\,\%$) to the relative error on the absolute energy scale arises from the limited statistics of neutrino-induced reference showers in the front part of the calorimeter where the test-beam events were located. Combined with other minor sources, the systematic error on the energy scale adds up to about 7 %.

6 Calibration of the scintillators

The scintillators of the target calorimeter had been in use since 1978 in an earlier CHARM experiment [1] where their main purpose was the determination of shower energies in sampling steps of one radiation length. In the larger CHARM-II detector, the scintillator layers were separated by 2.5 radiation length, and their use was restricted to the separation, in a sample of events, of electron-induced showers starting with a single electron track from π^0-induced background showers which start with an even number of tracks.

The response of the scintillator system to cosmic rays was monitored in roughly monthly intervals. It turned out that the average light attenuation factor, as measured over a length of 2.4 m, increased linearly with time from a factor 1.6 when the scintillators were first used in 1978 [2] to 4.5 at the start of CHARM-II in 1986, and to 6.5 at the end of 1990.

The original plan to use the shower response in scintillators as a reference to transport calibration results from the front end to the bulk of the calorimeter was dropped, because the methods based on the normalized hit multiplicity of the streamer tube system (section 4.1) and the use of neutrino induced showers for the system of pick-up strips (section 5.2) gave superior results. The inferiority of scintillators was due to the fact that the sampling steps, one scintillator layer per 2.5 radiation lengths, were too coarse compared to the shower evolution in the region covered by the test beam. Since the test-beam setup did not forsee the possibility of a longitudinal shift of the impact point by more than half a radiation length, it was not possible to average over all vertex positions modulo the sampling steps.

7 Angular resolution for electron showers

The determination of the shower direction is closely connected to the determination of the event vertex. Two algorithms are used:

The *maximized road* algorithm combines the search for the event vertex with the reconstruction of the shower axis. A first approximation for the axis is obtained from the digital data. After removal of isolated hits far away from the shower, this axis is obtained as a straight line fitted to the mean positions of hits in each tube layer and the vertex is defined as the intersection of this axis with the first tube layer of the shower. In a second step, the tube hits are weighted with the pulse height on the corresponding pick-up strip. In order to suppress noisy analog channels, the analog information is validated by comparison with the hit pattern in neighbouring tube layers. Combining both the digital and the analog data improves the vertex and direction estimate. Finally, the shower axis is determined in both projections by using the vertex as a pivot to rotate the axis through the shower, maximizing the number of hits in a narrow band ('road') centered on the axis. In this procedure each hit is attributed a weight according to a Gaussian function depending on the lateral distance from the axis.

This determination of the shower axis has been shown to give the best resolution for the shower direction. However, the algorithm is not fully efficient; it fails for 0.3 % of the events. In this case the *overall median* algorithm is used. It makes use of the vertex defined by the first step of the maximized road algorithm. Digital and analog data are used independently. Only tubes and pick-up strips closer than 10 cm to the first estimate of the shower axis are used. Furthermore in the longitudinal direction only activity within 90 % of the longitudinal

containment of the deposited energy is taken into account. For all activity inside this box, the angle between the line connecting it to the vertex and the detector axis is calculated. Weight factors depending on longitudinal and lateral position have been adjusted with the help of electron showers from the test beam. In the case of pickup strips, the position dependent weight is multiplied with the corresponding pulse height. The computed axis is the one which splits the shower, i.e. the sum of all weights, into halves. The final result is the average of the directions found from digital and from analog data. This algorithm is fully efficient, but the resolution is slightly worse than that of the maximized road.

The angular and the vertex resolutions, displayed in fig. 15 are obtained from the test beam. The improvement of the vertex resolution at higher energies, is a consequence of combining the vertex search with the direction finding. Above 12 GeV a resolution of ± 2.3 mm was found.

The resolution for the projected angle of electron showers in the energy range from 2 to 40 GeV can be parametrized by combining three terms:

$$\left[\frac{\sigma(\theta_{\mathrm{proj}})}{\mathrm{mrad}}\right]^2 = \left[\frac{2.25}{\log_{10}(E_e/\mathrm{GeV})}\right]^2 + \left[\frac{14.5}{\sqrt{E_e/\mathrm{GeV}}}\right]^2 + \left[0.03 \cdot \frac{E_e}{\mathrm{GeV}}\right]^2 \quad (12)$$

The first term is due to the finite vertex resolution. It depends on the distance between vertex and shower center, and thus shows a logarithmic dependence on the shower energy. The second term is due to particle statistics in the shower and the third term accounts for saturation effects in the shower core.

The angular resolution measured in the test beam needs a small correction before it can be applied to neutrino-electron scattering events. Due to variations of the response function along the calorimeter, the angular resolution averaged over the full calorimeter is slightly worse. To account for this, a random fluctuation was superimposed to the strip charges which were measured in the test beam. The amount of this variation was deduced from a study of the distribution of the pickup charges when exposed to cosmic-ray muons. This procedure led to a slightly modified resolution function (dashed curve in fig. 15):

$$\left[\frac{\sigma(\theta_{\mathrm{proj}})}{\mathrm{mrad}}\right]^2 = \left[\frac{2.64}{\log_{10}(E_e/\mathrm{GeV})}\right]^2 + \left[\frac{15.0}{\sqrt{E_e/\mathrm{GeV}}}\right]^2 + \left[0.03 \cdot \frac{E_e}{\mathrm{GeV}}\right]^2 \quad (13)$$

At 10 GeV, the mean energy of electrons in this experiment, the resolution is $\sigma_{\mathrm{proj}} = 5.4$ mrad.

8 Electron-hadron separation

8.1 Event selection

The initial step in the selection of neutrino-electron scattering candidates is a fast event recognition and hadron rejection without reconstruction of kinematic variables. It uses digital information of the streamer tubes only.

A shower is accepted if at least 30 hits are found in a range of at least 10 active tube layers, with not more than 7 consecutive non-active tube layers in between. Events with an outgoing muon are rejected by the requirement that there are not more than 60 active tube layers. These selection criteria are fully efficient for electrons with energies above 1.5 GeV.

In a first step of electron-hadron separation, four algorithms are applied:

1. The *digital road* algorithm is based on a comparison between the energy deposited in a narrow region around the shower axis and the total shower energy. For a preliminary determination of the shower axis, the medians of the deposited energy in each tube layer are used. Only activity within the 5th plane and the 20th plane after the event vertex is included:

$$R_{\mathrm{dig}} = \sum_{i=5}^{20} (N_{\pm 10\mathrm{cm}})_i \; / \sum_{i=5}^{20} (N_{\mathrm{tot}})_i \quad (14)$$

   where $N_{\pm 10\mathrm{cm}}$ is the number of active streamer tubes within ± 10 cm of the median and N_{tot} is the number of all active streamer tubes in the same layer (i).

2. In order to calculate the *80%-width* separator, one determines in each individual tube layer the hit distribution with respect to the median position of hits in this particular layer. All these distributions are then superimposed and the width which remains after cutting 10% of the hits from each tail is the 80%-width separator.

3. The *holicity* algorithm makes use of the fact that electromagnetic showers are more regular and dense than hadronic showers. Holicity is defined as

$$\chi^2_{\mathrm{hole}} = \sum_{i=3}^{12} \left(\frac{n_i^{\mathrm{hole}} - \langle n_i^{\mathrm{hole}} \rangle}{\sigma_i^{\mathrm{hole}}} \right)^2 \quad (15)$$

   where n_i^{hole} is the number of non active streamer tubes (holes) detected between the two outermost streamer tubes hits in tube layer (i). The quantities $\langle n_i^{\mathrm{hole}} \rangle$ and σ_i^{hole} denote the average number of holes and its standard deviation respectively and are determined from test-beam electron events.

4. The fourth algorithm is based on the graph theoretical concept of a *minimal spanning tree*. It tries to interconnect a given set of points (nodes) in a multidimensional space with the shortest possible network of direct links. This approach is described in detail in [7].

All four selection algorithms are strongly correlated. Each one alone can give a very good electron-hadron separation if the cuts are sufficiently strong. Only the combination of the four separators allows, however, to loosen the cuts to such an extent that electronmagnetic showers are retained with an efficiency of 99.6%, while hadronic showers are rejected with rejection factor of 27.

More refined algorithms reduce the background of hadronic events further. They make use of vertex and direction determinations described above. The selection is performed in three steps:

1. *Rejection because of tracks or of back scattering:*
   (a) Single tracks emerging from the vertex with an angle larger than 18° with respect to the shower direction suggest a hadronic process.
   (b) Long tracks emerging from the shower core give evidence for hadronic activity inside the shower.
   (c) More than two streamer tubes hit upstream of the vertex are regarded as backscattering from a semi-leptonic reaction.

2. The *combined road* algorithm: this algorithm is similar to the digital road algorithm. Here, the shower is longitudinally divided into a vertex region and a shower core region, and laterally into six subregions which allow the formation of a narrow road and of a broad road. Tube hits and strip charges are summed up for each region. The selection of the events is based on the symmetry of the lateral energy deposition and on the fractions of the deposited energy contained in the two roads. All quantities are calculated separately for digital and for analog data, for the two projections, and for the vertex and the shower core region. Comparison with results from test beam data leads to a decision of rejecting or retaining the event.

3. The *hit multiplicity* in the vertex plane (1-hit cut): The most severe cut applied in the selection of electron events is the requirement of exactly one streamer tube hit in the first active tube layer of the shower. This cut rejects about 16% of the neutrino-electron scattering events, but more than twice this fraction of background events.

8.2 Electron efficiency determination

The first selection step for neutrino-electron scattering candidates is the trigger decision. For the determination of the nominal trigger efficiency, i. e. assuming perfect hardware performance, a software simulated trigger is applied to test-beam electron events. Test-beam particles hit always the same part of the detector. To avoid a bias, the observed showers have been artificially moved through the detector before applying the software trigger. The trigger is fully efficient above 3 GeV, and the efficiency drops slowly at energies above 30 GeV (fig. 16).

To study the effect of hardware failures, a sample of events taken with lower trigger thresholds was used to derive effective threshold functions for each of the single trigger input signals. These threshold functions were then used and combined in the application of the software trigger to test-beam events.

The selection efficiency for neutrino-electron scattering events includes all selection algorithms applied in the off-line analysis, except the 1-hit cut, which will be treated separately. A study with test-beam electrons of different energies showed that the selection efficiency was essentially independent of energy (see fig. 17). Weighted with the energy spectra of neutrino-electron scattering events, the average selection efficiency is

$$\epsilon_{\mathrm{sel}} = 0.947 \pm 0.003_{\mathrm{stat.}} \pm 0.017_{\mathrm{syst.}} \qquad (16)$$

The systematic error arises from a small dependence of ϵ_{sel} on the vertex position in the calorimeter due to cross talk effects in the streamer tubes and from a very small dependence on the applied tube voltage.

The selection efficiency of the 1-hit cut depends on the early development of the shower, on the geometrical acceptance, on the response of the streamer tubes, on the tube voltage used during data taking and on the lateral position of the vertex. The first streamer tube layer following the glass plate in which the neutrino reaction has taken place can be inefficient. This happens if the electron traverses a tube layer entirely inside a wall which separates two streamer tubes, and is therefore not detected. The vertex algorithm will thus only find the vertex one plane later. The 1-hit efficiency accounts for this effect. Fig. 18 shows the hit multiplicity in the first streamer tube layer for test-beam electrons.

For all selection efficiencies one also has to consider a possible dependence on tube sensitivity and on cross-talk effects. In the case of the 1-hit cut both effects are significant and contribute to the systematic error. The resulting error of the 1-hit efficiency, obtained from test-beam data, contains an explicit dependence on the effective tube volt-

age:

$$\epsilon_{1\mathrm{hit}} = 0.804 \pm 0.003_{\mathrm{stat.}} \pm 0.022_{\mathrm{syst.}} + 0.03 \cdot \frac{\Delta U}{100\,\mathrm{V}} \quad (17)$$

with $\Delta U = < U_{\mathrm{eff}} > -4300\mathrm{V}$, where $< U_{\mathrm{eff}} >$ is the effective voltage defined in equation 2 and averaged over one year's data. The result is independent of the shower energy.

To apply the value of the 1-hit efficiency to neutrino data a small difference in the material traversed by the electron has to be accounted for. In the average, there are 0.23 radiation lengths between a neutrino-electron scattering vertex and the first streamer tube layer. Due to the monitoring equipment in the beam line, this quantitiy is increased to 0.26 radiation lenghts for test-beam events. To correct for this difference, test-beam data taken with additional material in the beamline are used. From fig. 19 one can read off the correction which has to be applied to the 1-hit selection efficiency:

$$\epsilon_{1\mathrm{hit}}^{\nu e} = \epsilon_{1\mathrm{hit}} + 0.034 \pm 0.012 \quad (18)$$

With the single contributions added in quadrature, the total systematic error of the electron selection efficiency amounts to 3.4 % of the final 1-hit efficiency.

9 Calibrations for muons

For the interpretation of the CHARM-II data, it is important to know the energy spectrum of the incoming neutrinos. This can be calculated from the momenta of muons which have been created by quasielastic neutrino scattering off nuclei. In this way, the calibration of the muon spectrometer sets, for the analysis of our data, the scale of neutrino energies.

9.1 Angular resolution for muon tracks in the calorimeter

The direction of muon tracks is determined in the target calorimeter from the digital information of the streamer tubes. A straight line fit, extending over 30 consecutive tube layers, takes into account space resolution and multiple scattering.

The resolution for the projected angle can be estimated to be

$$\left[\frac{\sigma_{\theta,\mathrm{proj}}}{\mathrm{mrad}}\right]^2 = \left[\frac{18}{(p/(\mathrm{GeV/c})^{3/4}}\right]^2 + 0.4^2 \quad (19)$$

where p refers to the muon momentum.

This has been experimentally verified with the use of long muon tracks, which were cut into two segments, and the direction of both segments was compared at the location of the cut. The resolution, determined from the observed differences, is in good agreement with this estimate (fig. 20).

9.2 Efficiency of the muon-spectrometer trigger system

The trigger for events with muons requires the response from at least 8 out of the first 16 scintillator layers in the muon spectrometer. Due to the large redundancy of the trigger, its efficiency could be deduced from the triggering events themselves. For each of the 768 scintillation counters, the pulse height distribution as a function of muon impact position and the minimal pulse height to produce a logic signal were determined from ADC and pattern unit information. This allows to calculate for a given track the probability that less than 8 discriminators gave signals and hence no trigger occurred.

The model was checked by comparing the predicted and the observed distributions for the number of active scintillator layers in a trigger (fig. 21).

The performance of the scintillators has gradually deteriorated with time. Compared with data taken in 1988, an increase of the effective thresholds by 12 % for the 1989 data and by 28 % for the 1990 data has been observed. Because of that, the trigger requirements have been relaxed from 1989 onwards to only at least 6 active scintillator layers.

The calculated inefficiencies, caused by the muon spectrometer trigger, is 2.16 % before 1989, 1.56 % in 1989 and 2.20 % in 1990. The error of the efficiency is mostly systematic and estimated to be ± 0.2 %.

9.3 Efficiency of track reconstruction in the spectrometer

The reconstruction efficiency for muons in the spectrometer has been studied with Monte Carlo events. The results have been corroborated with test beam muons.

The Monte-Carlo description of the data contains chamber efficiency, multiple scattering and energy loss with its fluctuations. Background hits, including their correlations with the muon track and within adjacent drift chamber gaps, are added according to distributions observed in the data. The reconstruction efficiency of Monte Carlo events varies slightly with muon momentum: it increases from 95 % at 5 GeV/c to a constant value of 98.5 % for momenta above 20 GeV/c.

Test-beam muons entering the calorimeter with 60 GeV/c lose on average 14.3 GeV/c before they reach the spectrometer with 45.7 GeV/c. The observed reconstruction efficiency for these muons is 97.4 ± 0.3 %.

9.4 Determination of muon momenta

Crucial for the reconstruction of the muon momentum in the magnetic spectrometer is an exact knowledge of the drift chamber positions. The chambers had been aligned by surveyers with 2 mm precision along the beam line and with 0.5 mm precision perpendicular to it. Using high energy muons

accompaning the neutrino beam the perpendicular alignment was improved to ± 0.2 mm.

As for the determination of the reconstruction efficiency, mainly Monte Carlo events were used to study the momentum determination. The result has been checked at 46 GeV/c with the use of test-beam muons.

For the spatial distribution of the magnetic field, a parametrisation derived by the CDHS group [8] was used, which locally reproduces the field to about 1 %. The integral in radial direction was checked experimentally with ± 0.6 % precision by measuring the time integral of the voltage induced in a pickup loop when reversing the excitation current.

Fig. 22 shows the relative momentum resolution and the relative bias as a function of muon momentum derived from Monte-Carlo events, the bias being the difference of the reconstructed minus the true momentum. For the bulk of our data, which have a mean momentum around 25 GeV/c, the resolution is 13 % with a bias of -2 %.

The predicted bias and the resolution have been verified with test beam muons of 60 GeV/c. Data have been taken with both signs of the excitation current (focussing or defocussing the tracks in the spectrometer). In the focussing mode, the data are reconstructed with 46.4 GeV/c mean energy at the entrance of the spectrometer, corresponding to 60.7 GeV/c at the upstream end of the target calorimeter, while for Monte Carlo muons of 60 GeV/c the values 45.7 and 60.0 GeV/c are obtained. The corresponding numbers for the defocussing mode are 46.0 and 60.3 GeV/c for the data and 46.3 and 60.6 GeV/c for Monte Carlo. The observed differences are consistent with the uncertainities of the test beam momentum (± 1 %), the field distribution(± 1 %), the field integral (± 0.6 %), and the statistical errors of the measurements (± 0.3 % for the data and ± 0.4 % for Monte Carlo).

We conclude that the scale of the momentum determination is known within ± 2 %.

The observed momentum resolution for test beam muons is reproduced to better than 10 % by the Monte Carlo calculation, as shown in fig. 23.

Acknowledgements

We gratefully acknowledge the skill and dedication of our many technical collaborators who have contributed to the realization and the operation of the detector and of its associated systems. The experiment has been made possible by grants from the Inter-University Institute for Nuclear Sciences (Belgium), CERN (Geneva, Switzerland), the Bundesministerium für Forschung und Technologie (FRG), the Institute of Theoretical and Experimental Physics (Moscow, Russian Federation), and the Istituto Nazionale di Fisica Nucleare (Italy); we gratefully acknowledge their support. We should like to thank L. Gatignon and his collaborators for his competent assistance ensuring the excellent performance of the CERN X7 test beam.

References

[1] CHARM-Collab., J. Dorenbosch et al., Nucl. Instr. & Meth. A 253 (1987) 203.

[2] CHARM-Collab., M. Jonker et al., Nucl. Instr. & Meth. A 200 (1982) 183.

[3] CHARM-II Collab., K. De Winter et al., Nucl. Instr. & Meth. A 278 (1989) 670.

[4] CHARM-II Collab., D. Geiregat et al., Phys. Lett. 259 B (1991) 499.

[5] CHARM-II Collab., P. Vilain et al., Nucl. Instr. & Meth. A 277 (1989) 83.

[6] CHARM-II Collab., P. Vilain et al., Phys. Lett. 281 B (1992) 159.

[7] CHARM-II Collab., K. De Winter et al., Nucl. Instr. & Meth. A 277 (1989) 170.

[8] CERN – Dortmund – Heidelberg – Saclay collaboration, private communication.

Figure captions

Figure 1: Overview of the CHARM-II detector. The veto system was removed during the test-beam operation.

Figure 2: Display of two test-beam events in one out of two available projections: (a) 10-GeV electron and (b) 10-GeV pion. The small dots represent tube hits, and the area of the squares is proportional to the pulse height on the pickup strips.

Figure 3: Layout of the test beam as seen from the top. P1 and P2 are the two points of impact of the beam on the calorimeter.

Figure 4: Dependence of the hit multiplicity on the absolute value of the slope of the muon track, measured in a plane perpendicular to the wire. No angular dependence is observed in the other projection.

Figure 5: Dependence of the hit multiplicity on the coordinate along the wire. The positive end of the abscissa corresponds to the read-out end of the wire.

Figure 6: Dependence of the normalized hit multiplicity on the tube voltage. The straight line represents eq. 2.

Figure 7: Effective streamer tube voltage as a function of time. Each entry corresponds to one calibration period. Only data-taking periods are shown. The distance between marks on the abscissa is one month. (The detailed study of the response behaviour discussed in section 4.1 had been triggered by the discovery of the high fluctuations in 1988.)

Figure 8: Effective streamer tube voltage as a function of the coordinate along the beam axis. Each entry represents a group of twenty modules.

Figure 9: Number of tubes hit by an electromagnetic shower as a function of energy. The curve represents the fit function given by eq. 3.

Figure 10: The number of active tubes per GeV as a function of the pion energy.

Figure 11: Variation of the charge from the pickup strips as a function of the relative position within the modular structure of the streamer tube layers.

Figure 12: Variation as a function of the current strip number within one selected tube layer: (a) raw charge from the pickup strips before and (b) corrected charge after the strip-by-strip and tube-by-tube calibration .

Figure 13: Total charge (sum of ADC-counts) on the pickup strips for electromagnetic showers as a function of the test-beam energy. The curve fitted to the data is given by eq. 9.

Figure 14: Overall resolution function for the energy determination of electromagnetic showers using the charges on the pickup strips. Intrinsic errors due to shower fluctuations in the test beam are combined with the errors due to the propagation of the calibration from the test beam to the rest of the detector. The curve represents eq. 11.

Figure 15: The angular resolution (left) for test-beam electrons (solid curve, eq. 12) and for neutrino induced electrons (dashed curve, eq. 13). The right side shows the vertex resolution.

Figure 16: Trigger efficiency as a function of the electron shower energy.

Figure 17: Selection efficiency as a function of the electron shower energy.

Figure 18: Distribution of the hit multiplicity in the vertex plane of an electromagnetic shower.

Figure 19: Dependence of the 1-hit efficiency on the material in front of the first streamer tube layer.

Figure 20: Momentum dependence of the angular resolution for muon tracks in the target calorimeter. The line shows the Monte Carlo prediction (eq. 19). The agreement between the data points for different years shows the stability of the detector.

Figure 21: Probability distribution for the number n of active scintillator layers, averaged over all muon events in the 1988 data. The Monte Carlo prediction is compared with the data which have been taken with the trigger condition $n \geq 8$.

Figure 22: Momentum resolution (a) and momentum determination bias (b) for reconstructed Monte Carlo events.

Figure 23: Distribution of momenta reconstructed at the entrance of the target calorimeter. The muons in the test beam had an average momentum of 60 GeV/c. The momentum bite of the beam was 3 %.

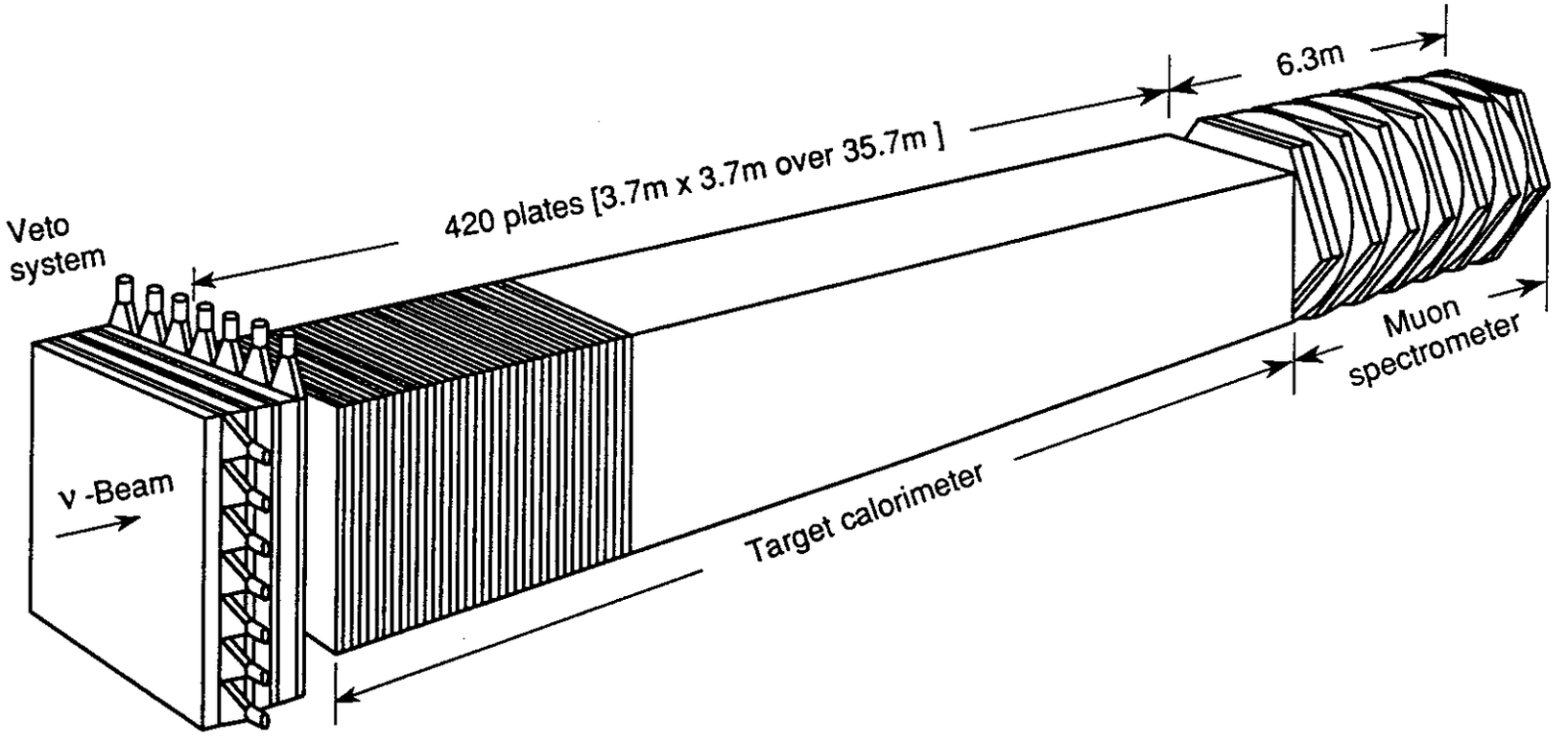
6.3m
420 plates [3.7m x 3.7m over 35.7m]
Veto
system
Muon
spectrometer
ν -Beam
Target calorimeter

Fig. 1

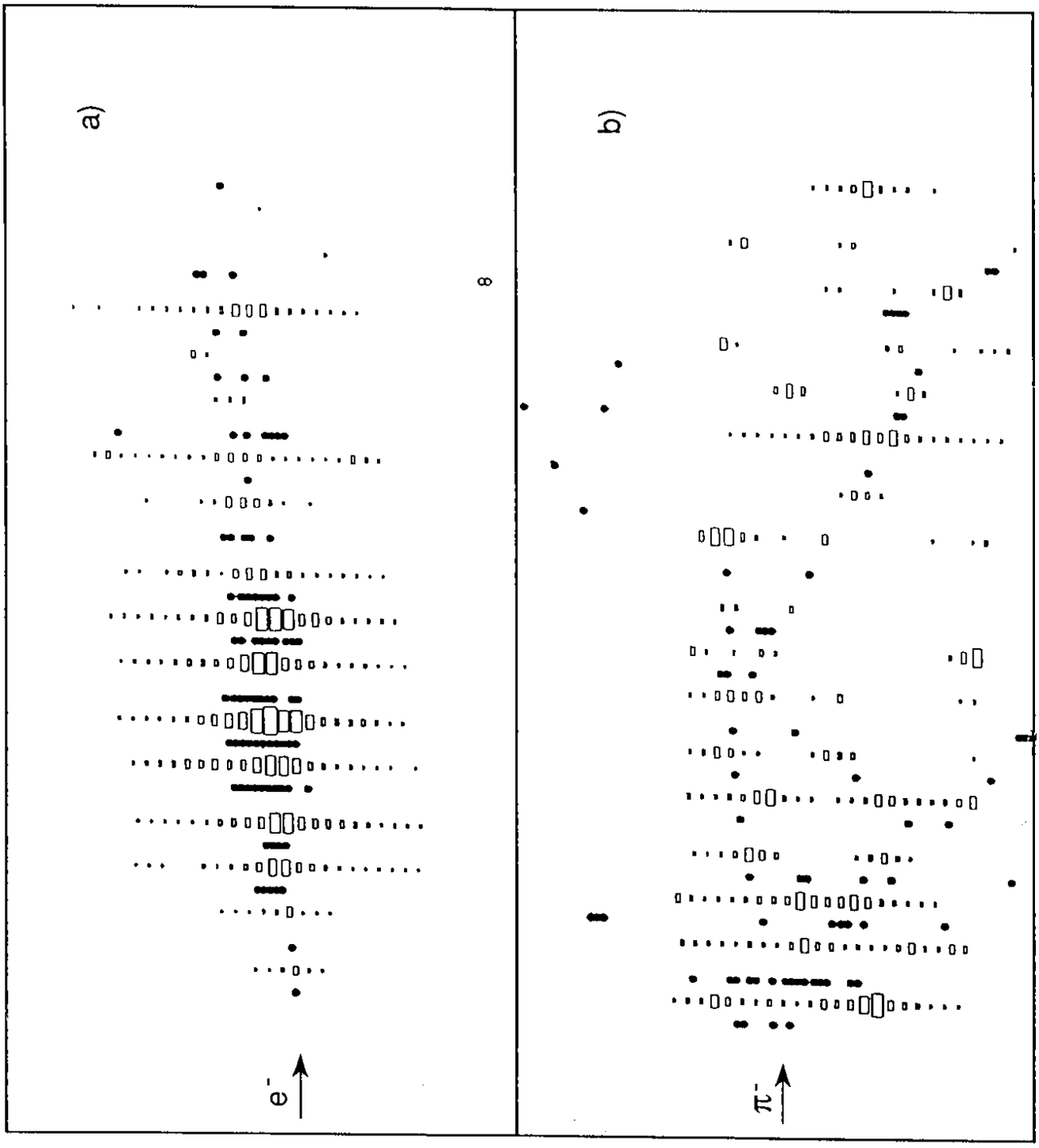

Fig. 2

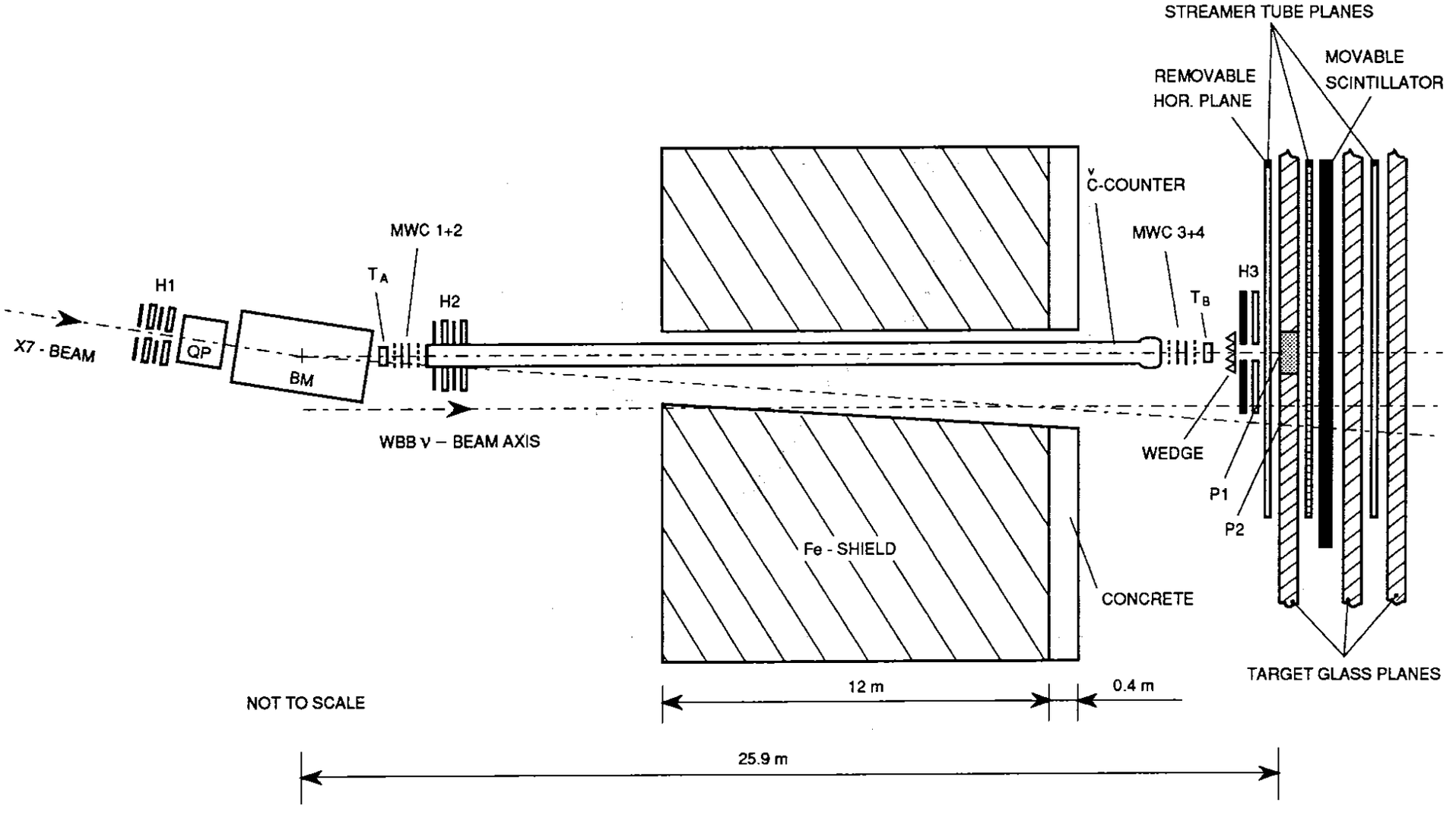
STREAMER TUBE PLANES
REMOVABLE
HOR. PLANE
MOVABLE
SCINTILLATOR
ν
C-COUNTER
MWC 1+2
MWC 3+4
H1
T_A
H2
H3
T_B
X7 - BEAM
QP
BM
WBB ν – BEAM AXIS
WEDGE
P1
P2
Fe - SHIELD
CONCRETE
TARGET GLASS PLANES
NOT TO SCALE
12 m
0.4 m
25.9 m

Fig.3

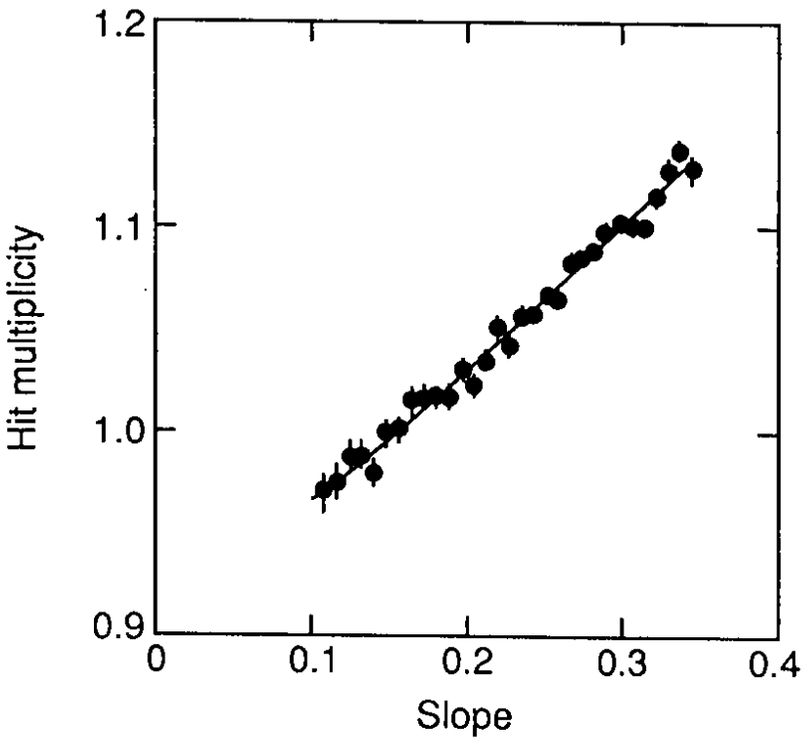

Fig. 4

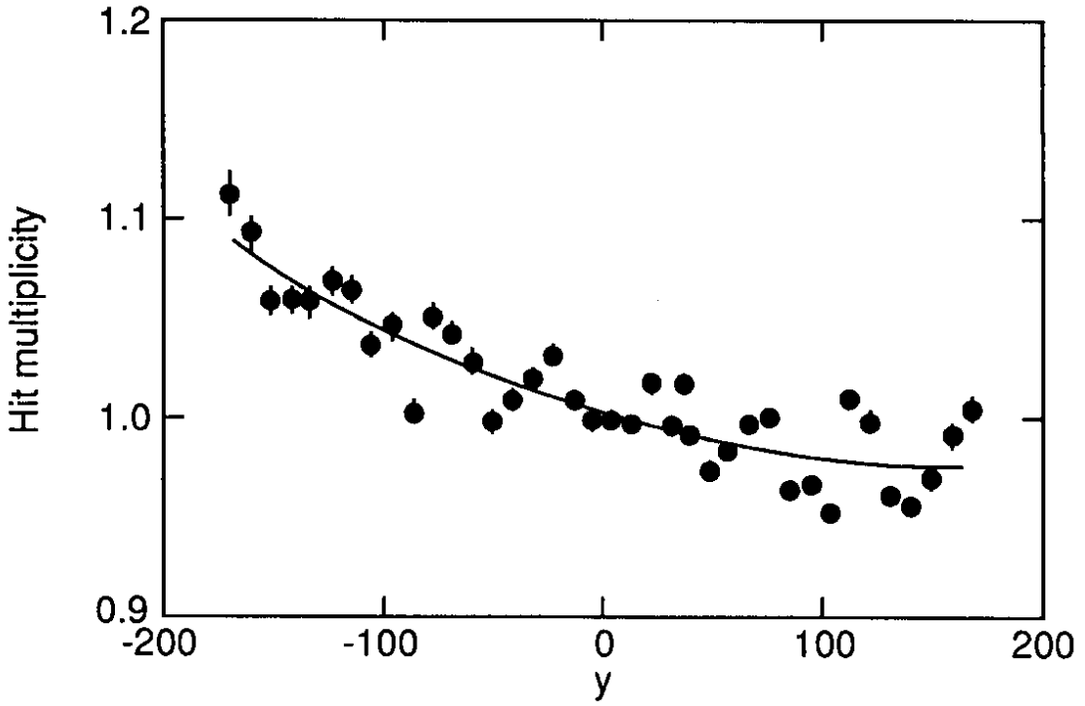

Fig. 5

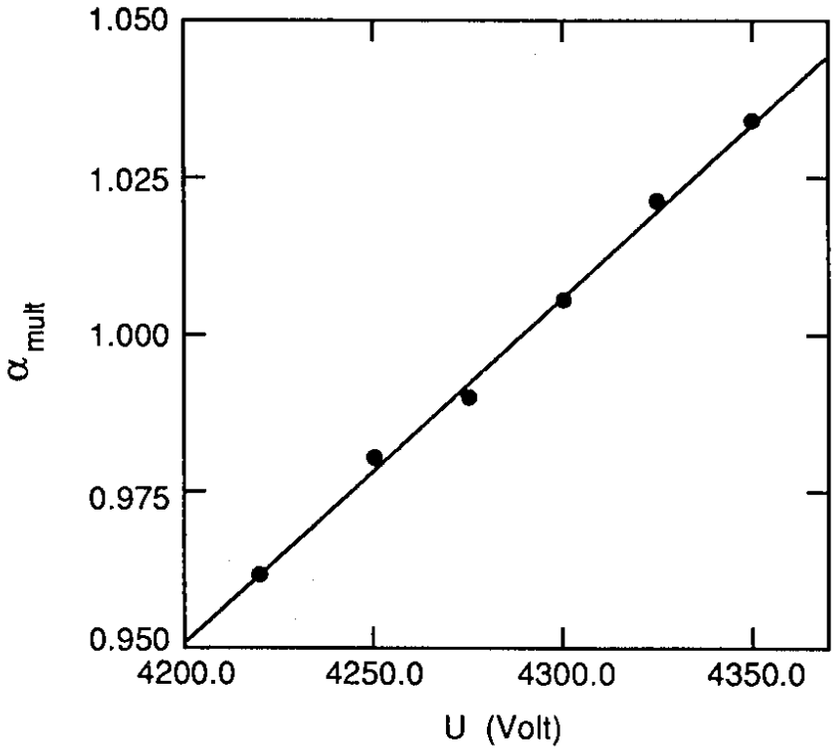
1.050
1.025
1.000
0.975
0.950
α_{mult}
4200.0
4250.0
4300.0
4350.0
U (Volt)

Fig. 6

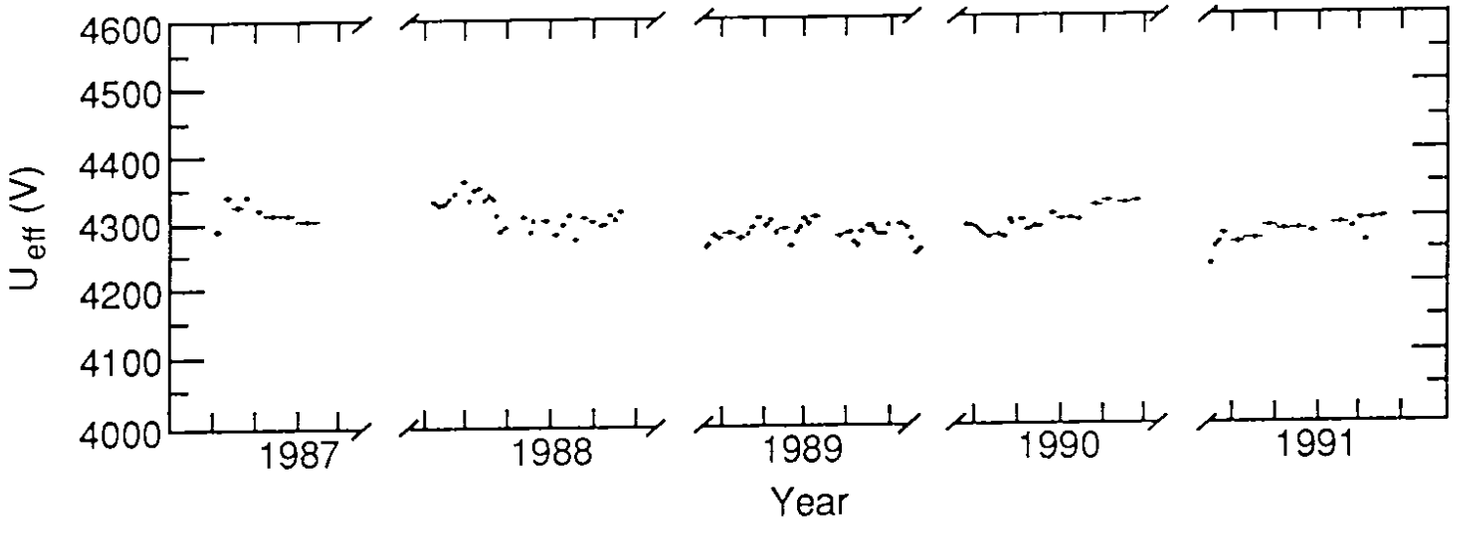
4600
4500
4400
4300
4200
4100
4000
U_{eff} (V)
1987
1988
1989
1990
1991
Year

Fig. 7

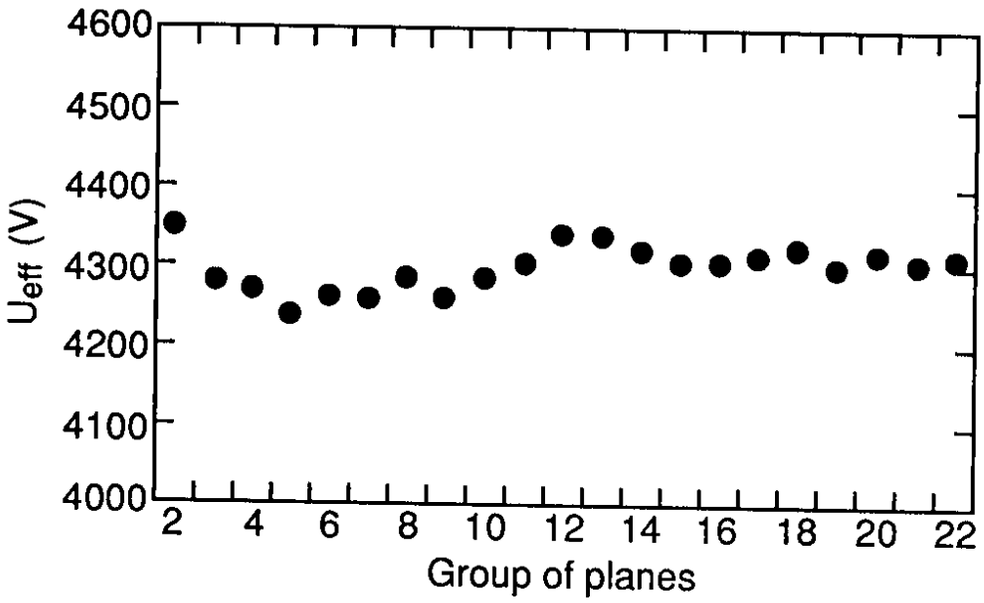
4600
4500
4400
4300
4200
4100
4000
U_{eff} (V)
2
4
6
8
10
12
14
16
18
20
22
Group of planes
Fig. 8

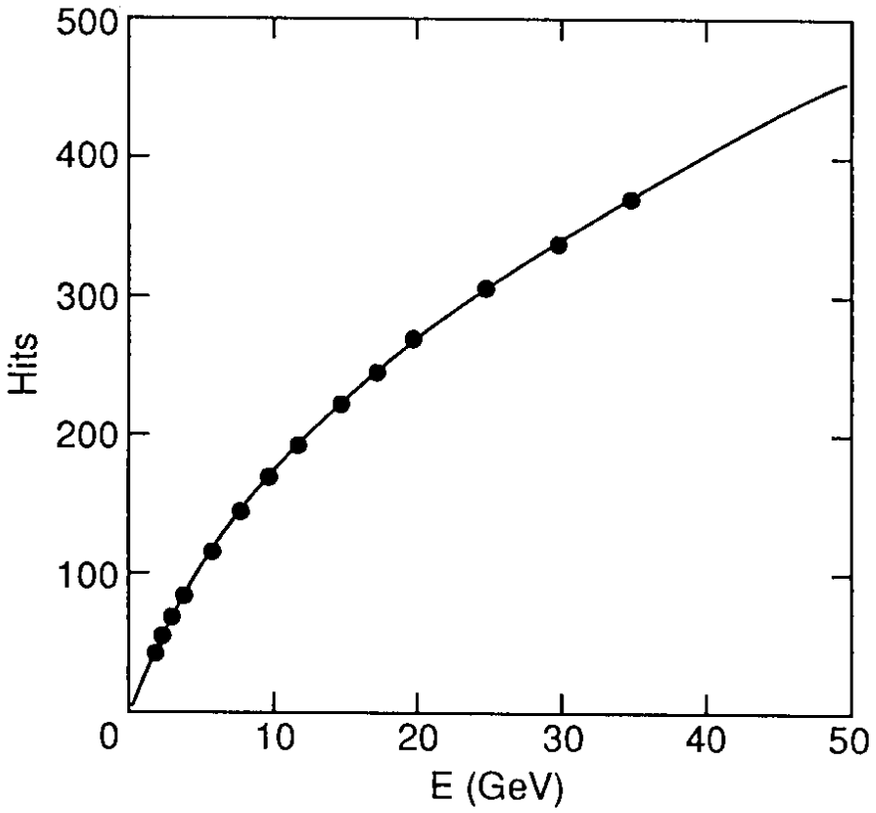

Fig. 9

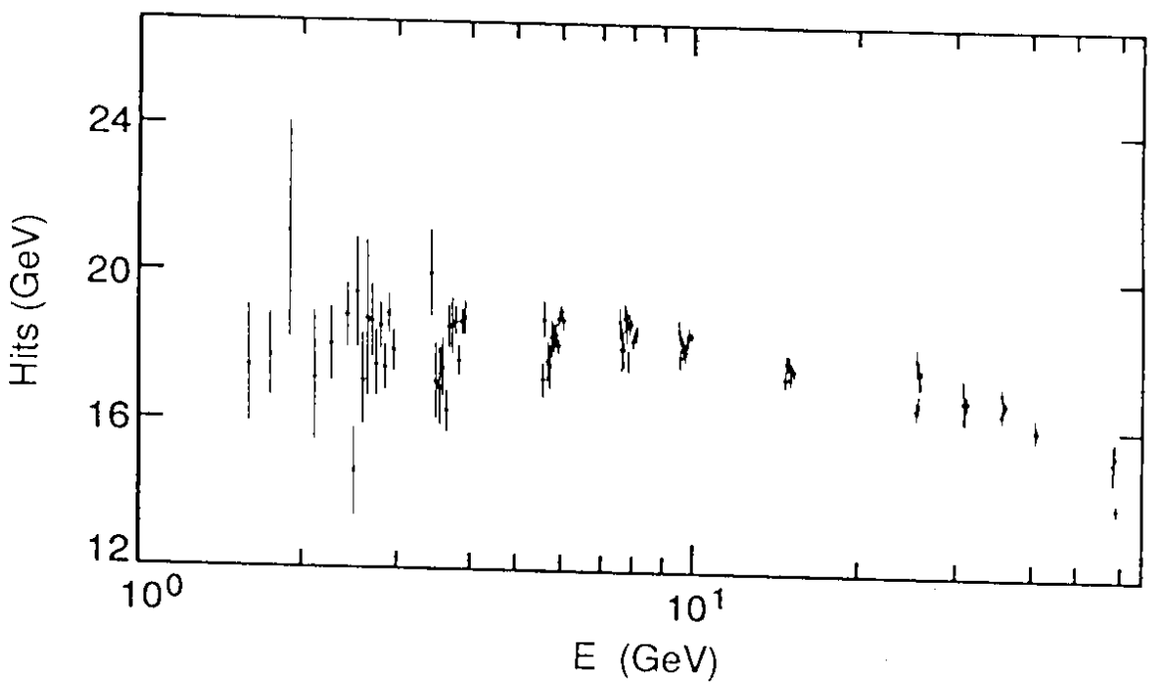

Fig 10

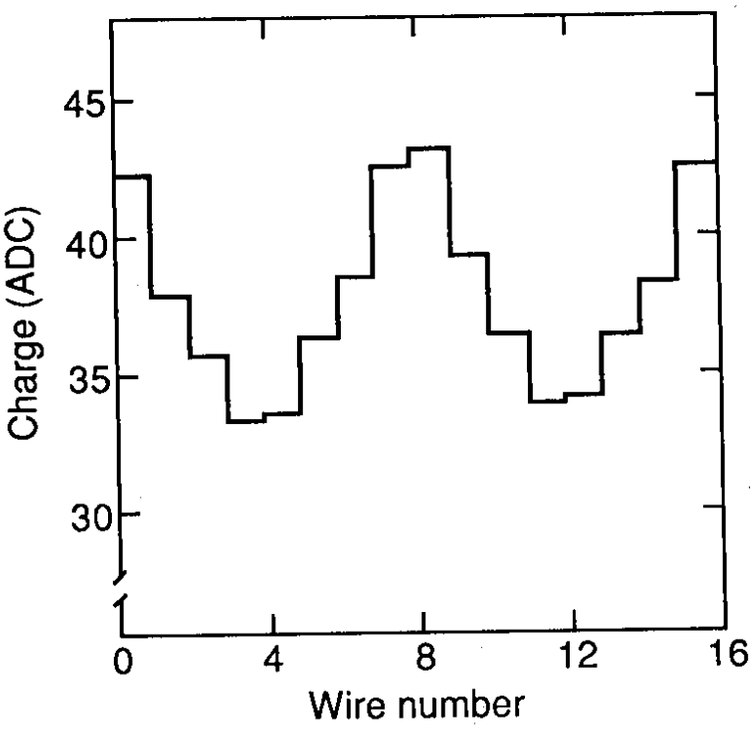

Fig. 11

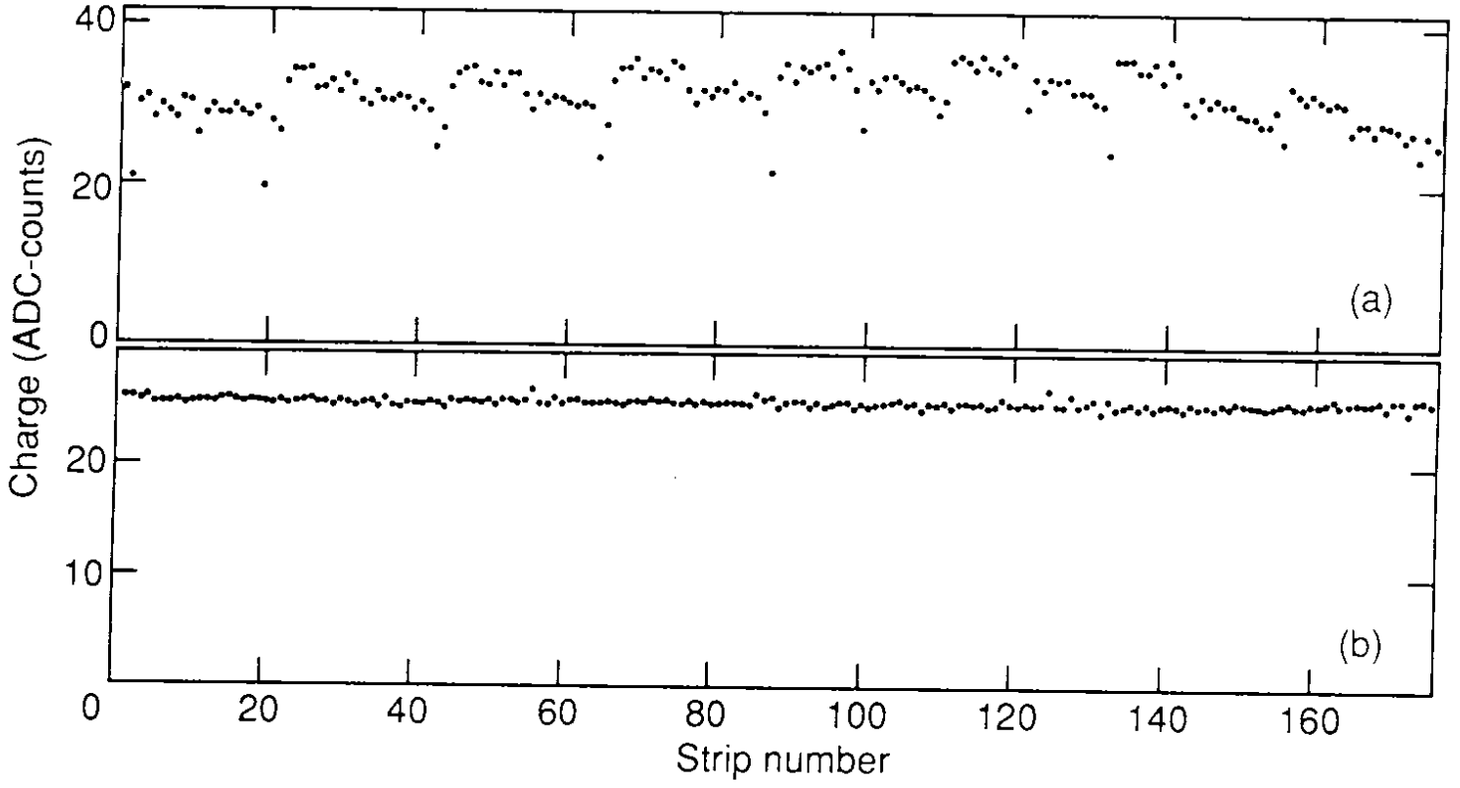
40
20
0
(a)
20
10
0
(b)
0
20
40
60
80
100
120
140
160
Charge (ADC-counts)
Strip number

Fig. 12

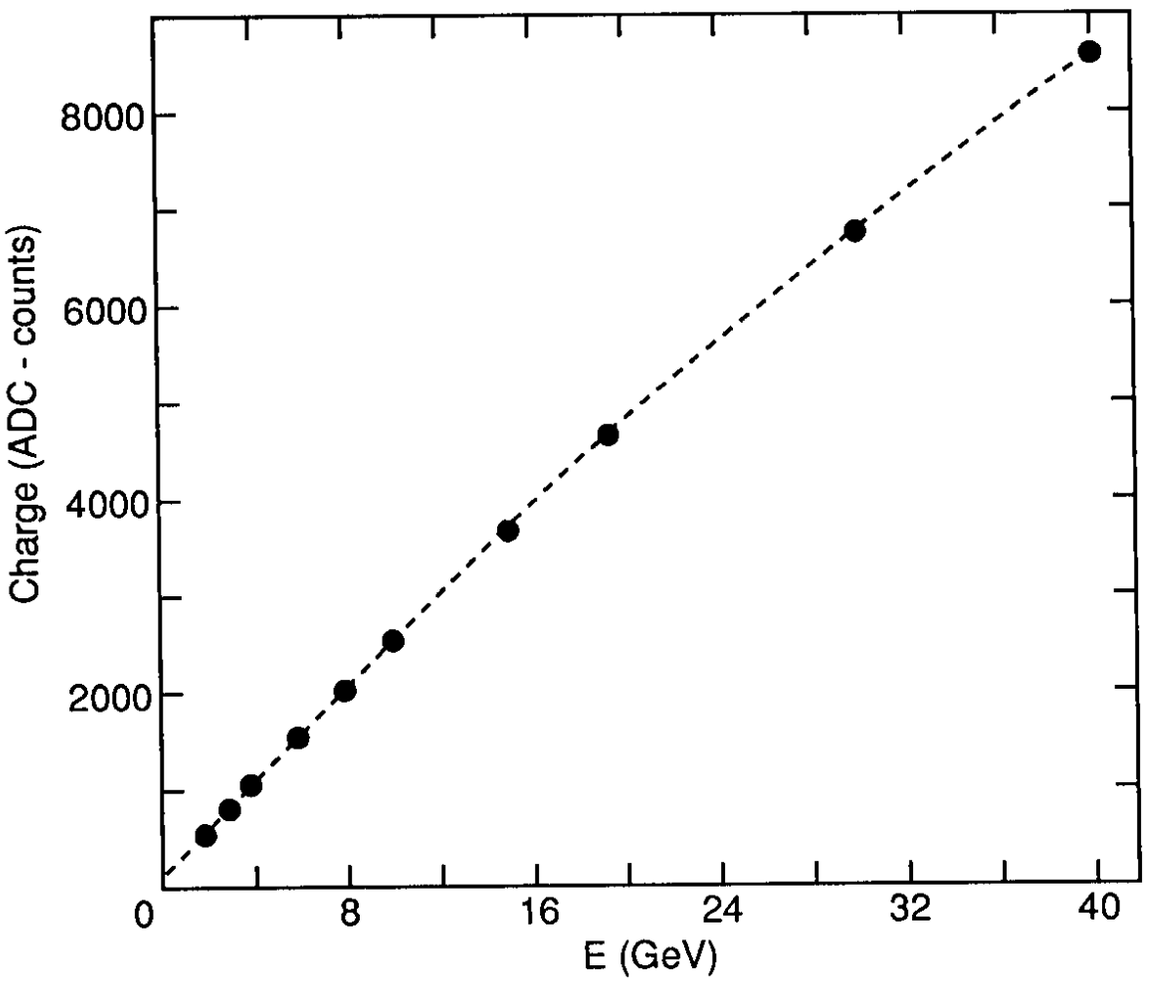

Fig. 13

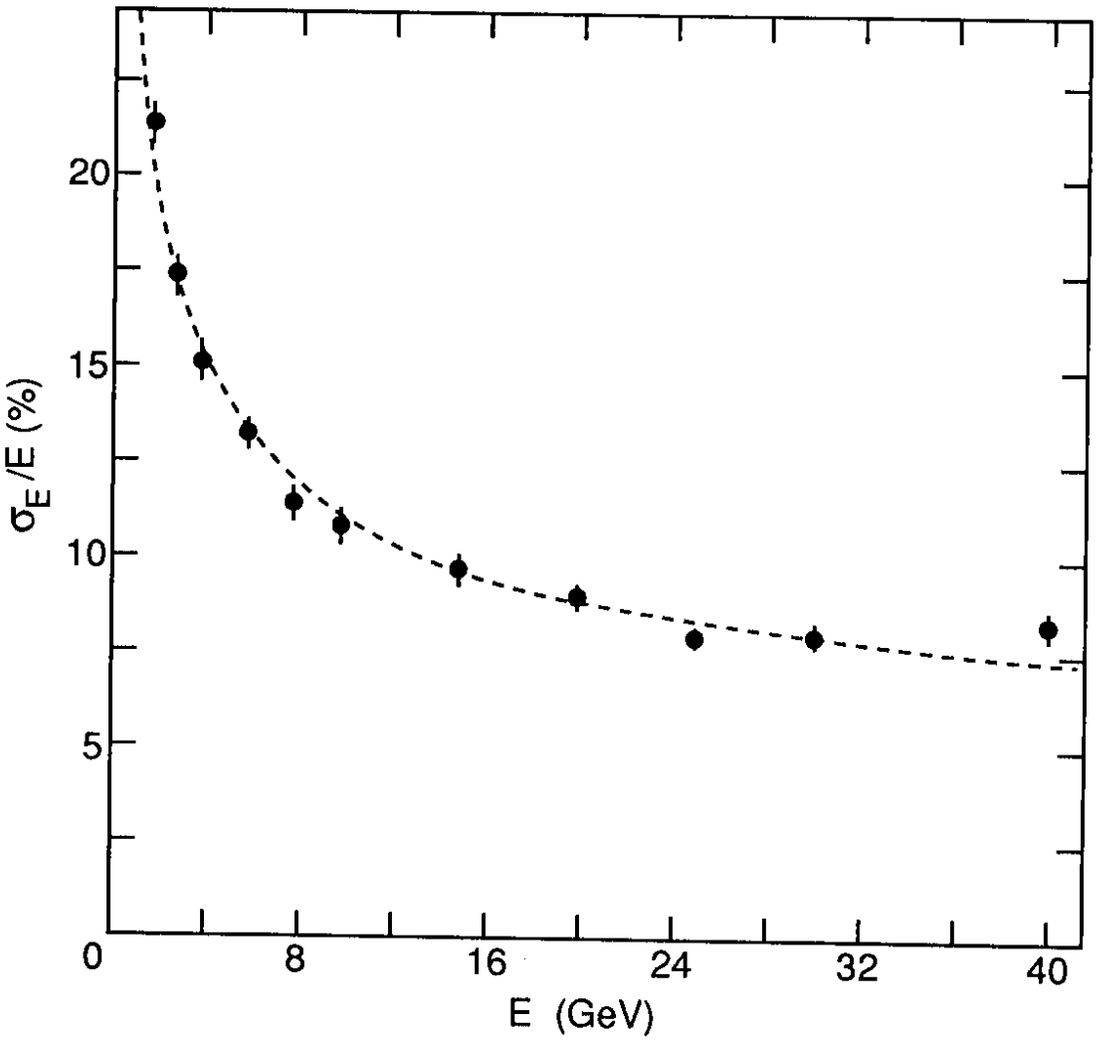

Fig. 14

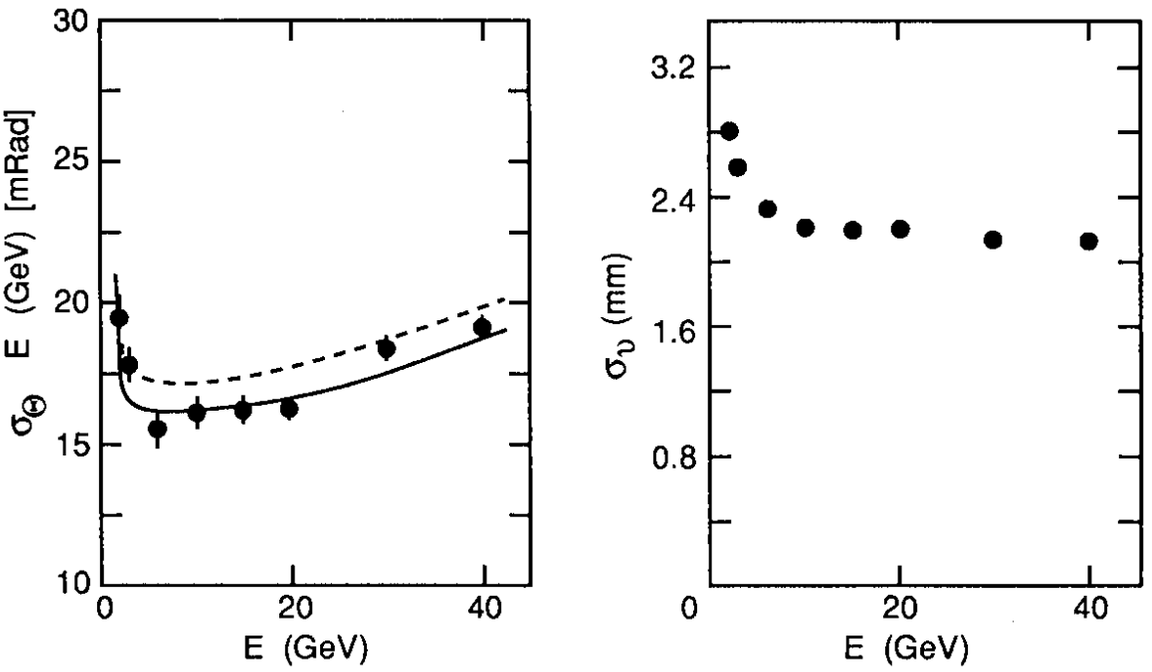
30
25
20
15
10
0
20
40
E (GeV)
σ_Θ E (GeV) [mRad]
3.2
2.4
1.6
0.8
0
20
40
E (GeV)
σ_υ (mm)

Fig. 15

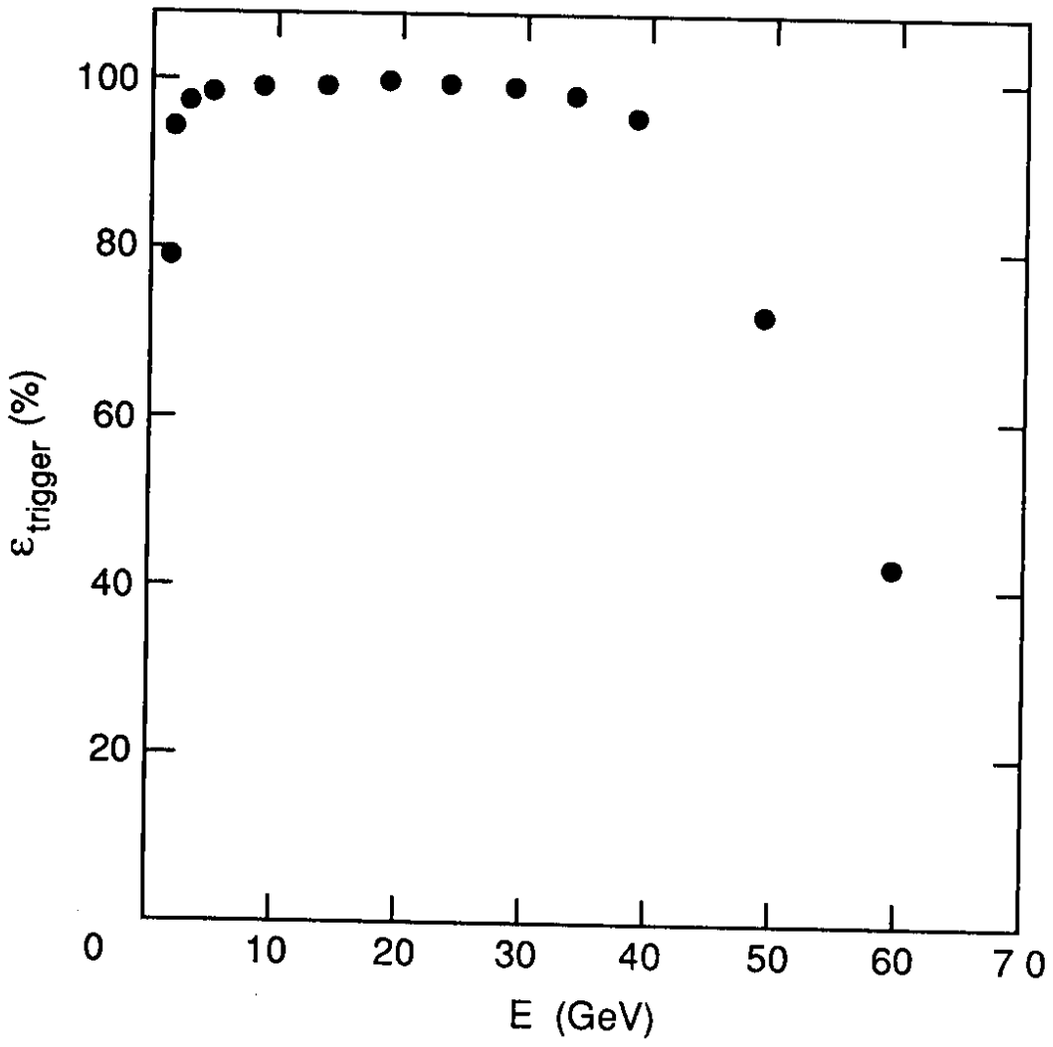

Fig. 16

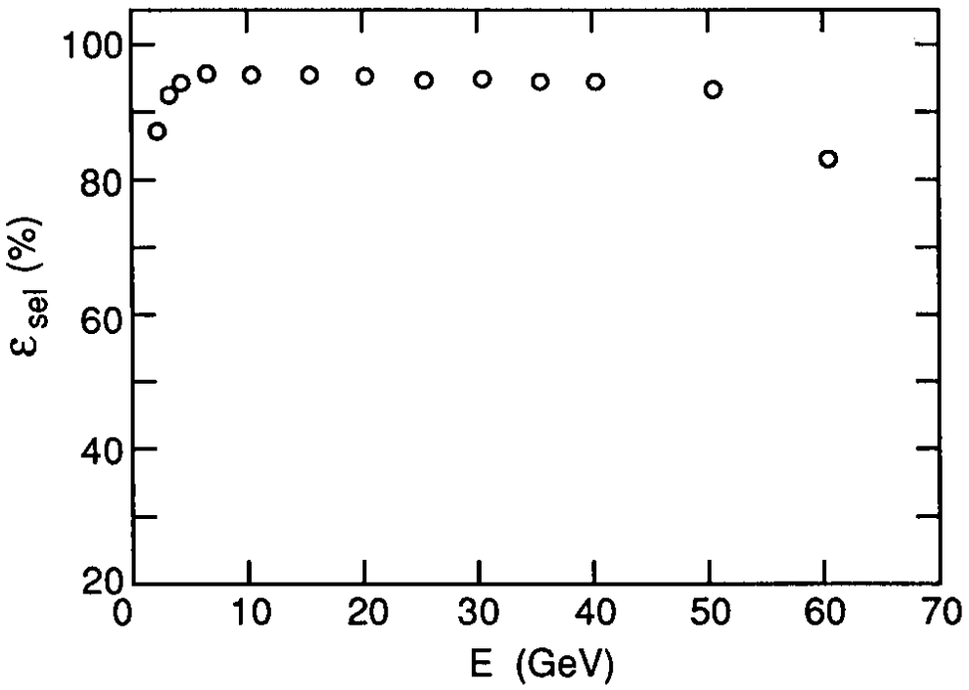

Fig. 17

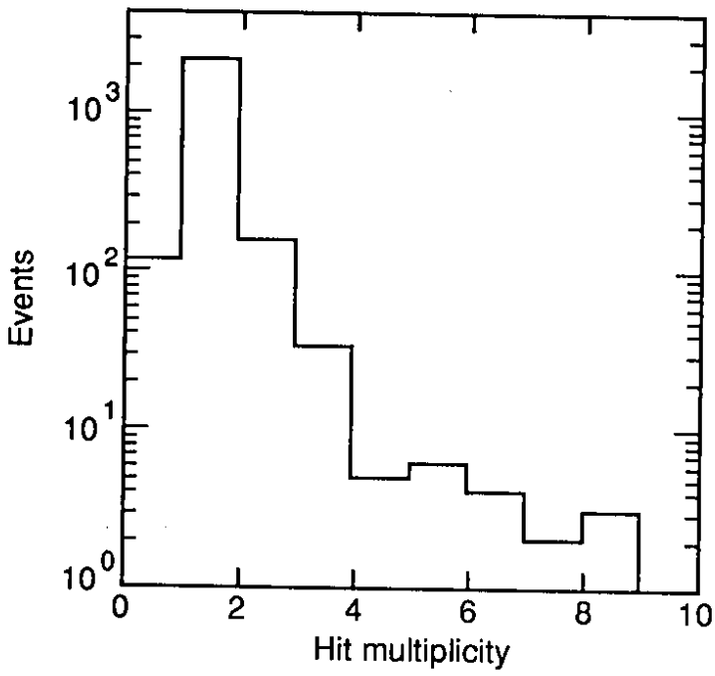

Fig. 18

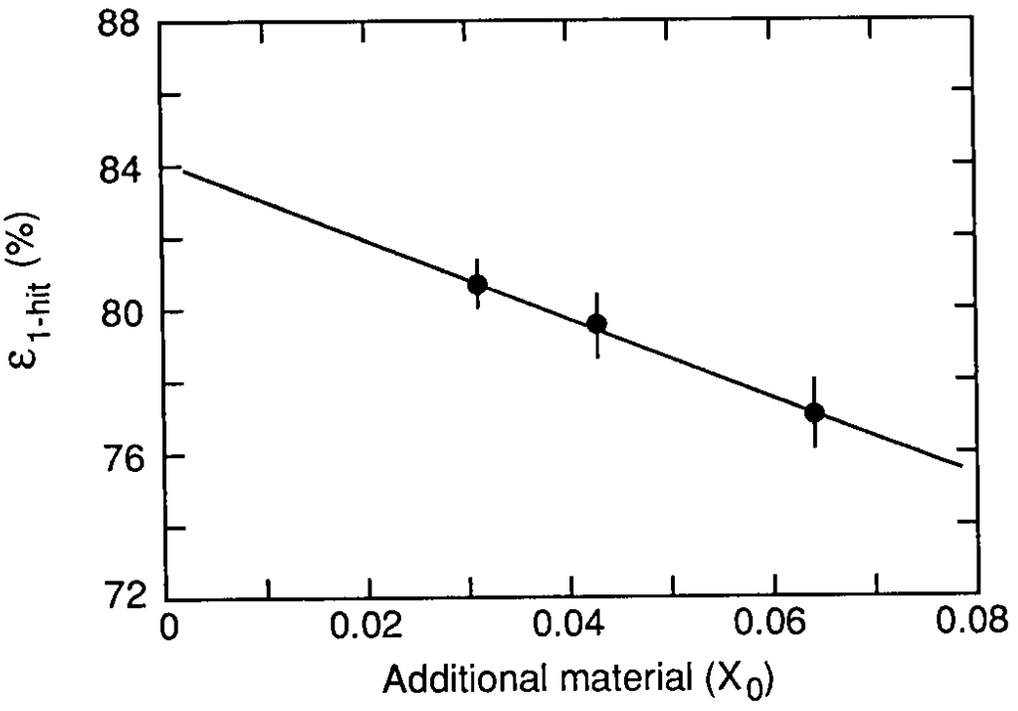
88
84
80
76
72
$\varepsilon_{1\text{-hit}}$ (%)
0
0.02
0.04
0.06
0.08
Additional material (X_0)

Fig. 19

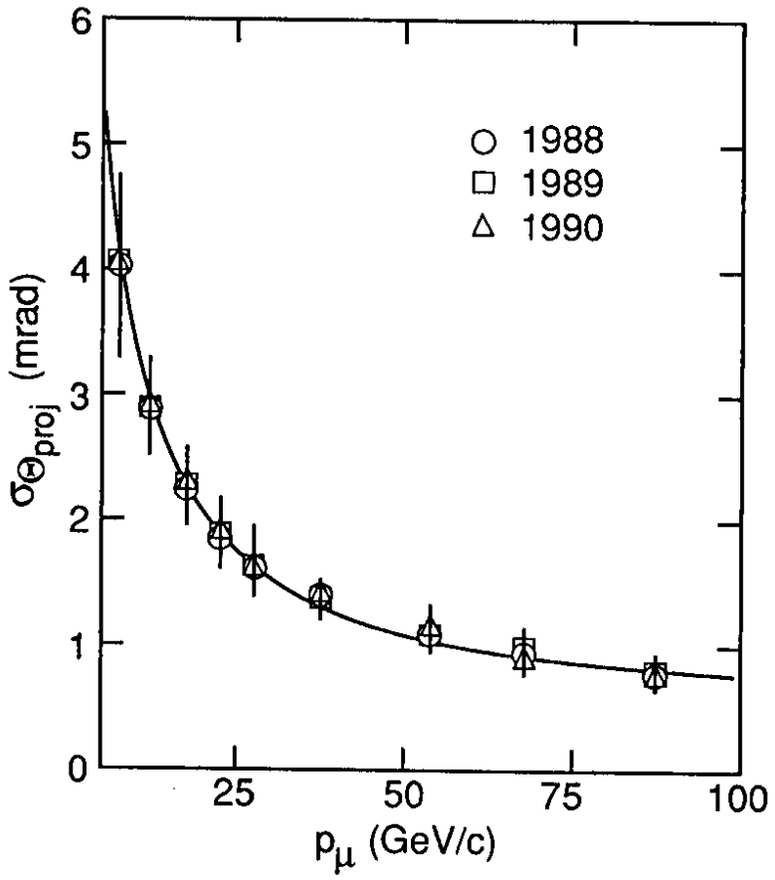
6
5
4
3
2
1
0
25
50
75
100
1988
1989
1990
$\sigma_{\Theta_{proj}}$ (mrad)
p_μ (GeV/c)

Fig. 20

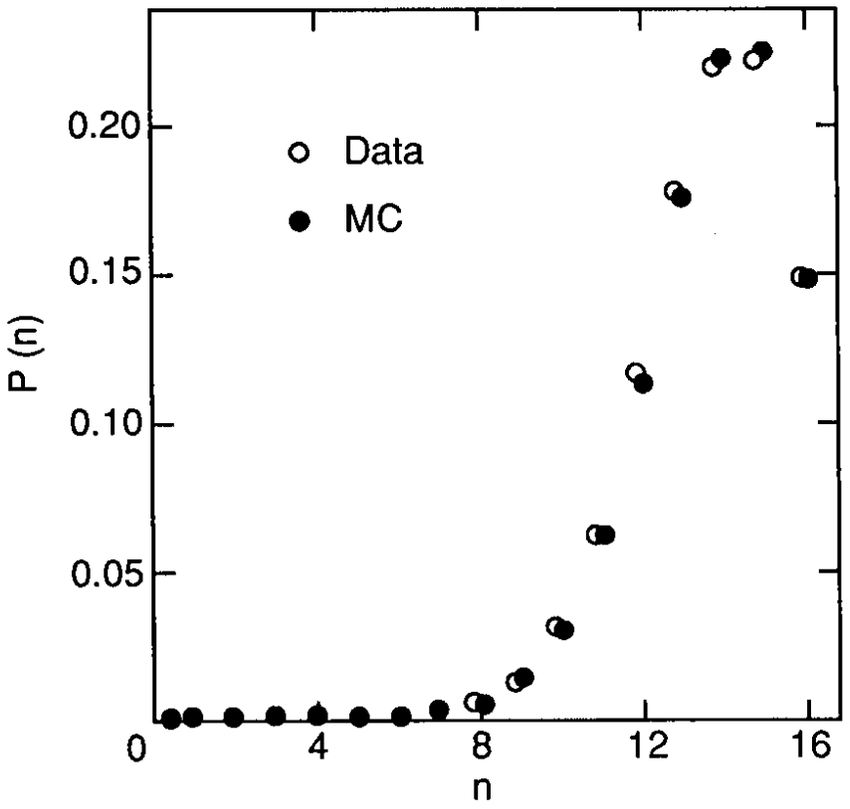

Fig. 21

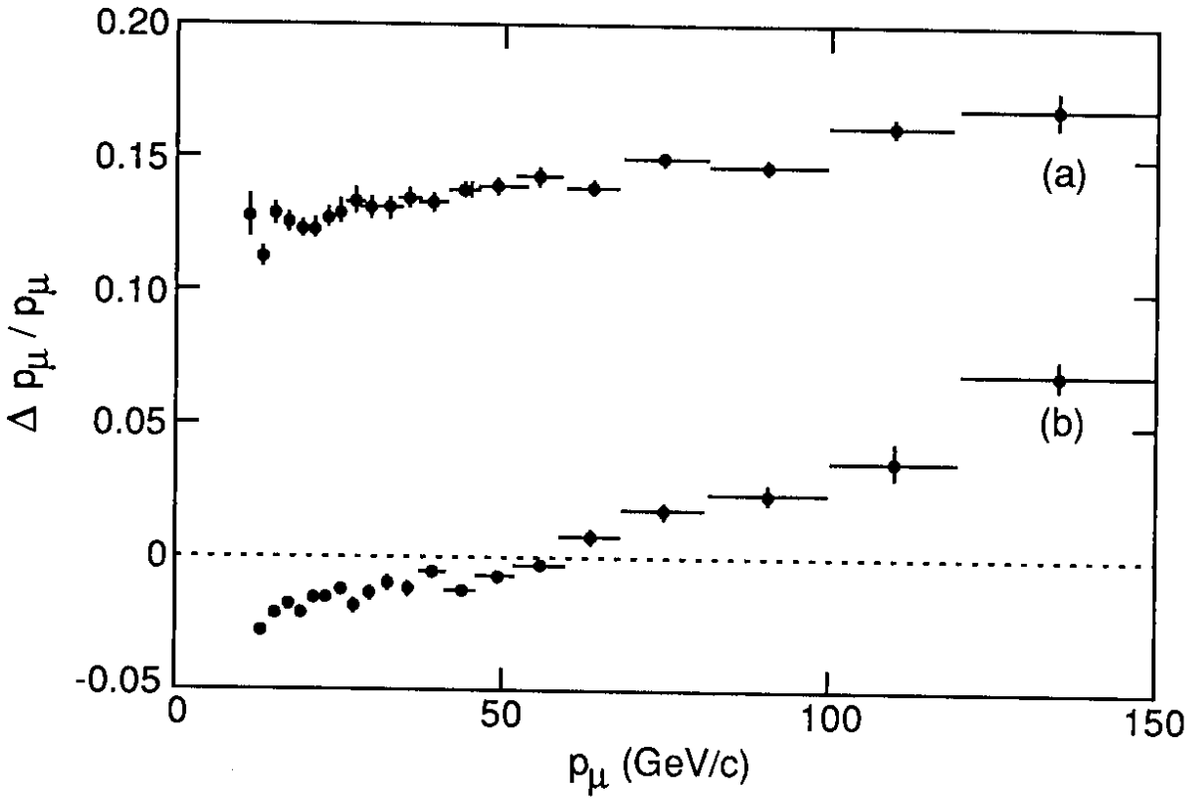

Fig. 22

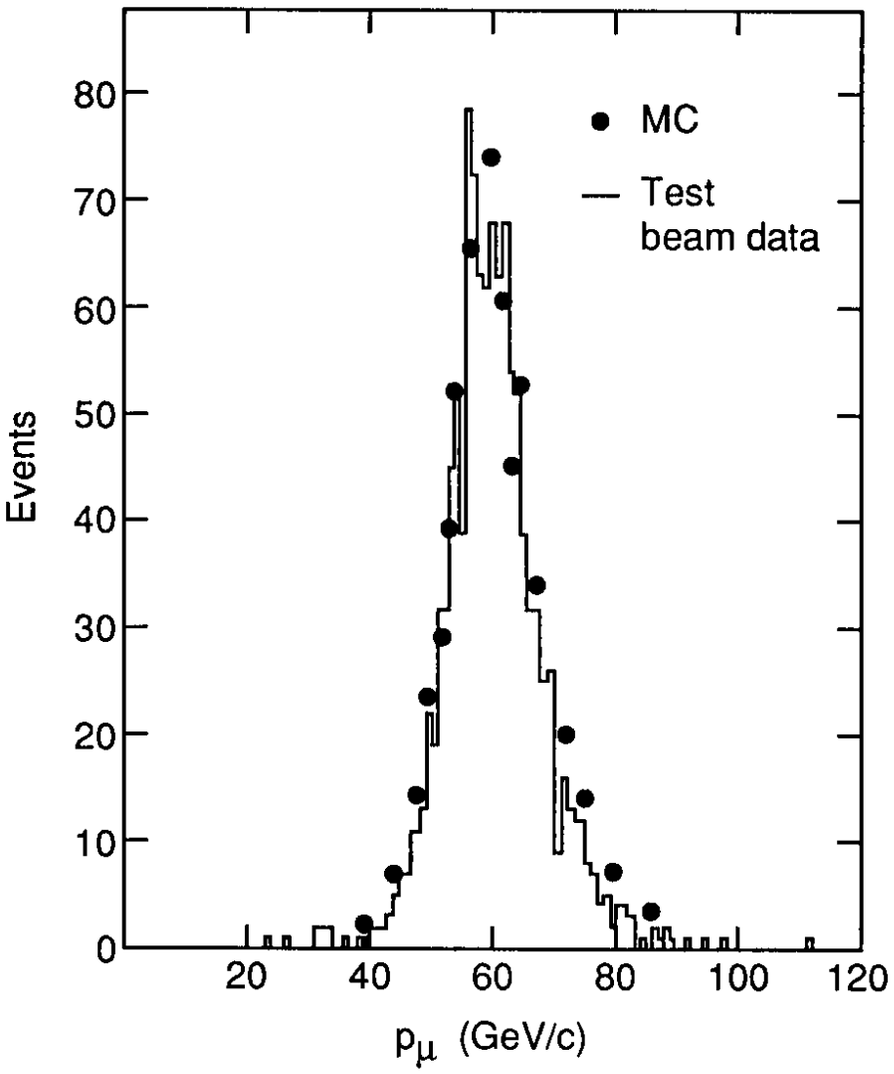
MC
Test
beam data
Events
0
10
20
30
40
50
60
70
80
20
40
60
80
100
120
p_μ (GeV/c)

Fig. 23